

CONFERENCES AND SYMPOSIA

PACS number: 01.10.Fv, **43.30. + m**, **43.60. + d**, 92.10.Ve; **12.20. – m**, 12.20.Ds, 31.30.Gs, 31.30.Jv; 06.20.Jr, 06.30.Ft, 12.20.Fv, 32.10.Fn, 32.30.Jc, 42.62.Fi

Selected problems in hydrodynamics, quantum electrodynamics, and laser spectroscopy (Scientific session of the Physical Sciences Division of the Russian Academy of Sciences, 14 May 2008)

V S Davydov; V M Shabaev; N N Kolachevsky

DOI: 10.1070/PU2008v051n11ABEH006643

On May 14, 2008 a science session of the Physical Sciences Division of the Russian Academy of Sciences (RAS) was held at the conference hall of the Lebedev Physical Institute, RAS. The following reports were presented at the session:

(1) **Davydov V S** (St. Petersburg Electrotechnical University, St. Petersburg) "Physical and mathematical foundations of the multialternative recognition and identification of hydrolocation fields produced by bodies of complex geometric shapes";

(2) **Shabaev V M** (St. Petersburg State University, St. Petersburg) "Quantum electrodynamics of heavy ions and atoms: current status and prospects";

(3) **Kolachevsky N N** (Lebedev Physical Institute, RAS and Moscow Institute for Physics and Technology, Moscow) "High-precision laser spectroscopy of cold atoms and the search for the drift of the fine structure constant."

Abridged versions of the above reports are given below.

PACS numbers: **43.30. + m**, **43.60. + d**, 92.10.Ve
DOI: 10.1070/PU2008v051n11ABEH006642

Physical and mathematical foundations of the multialternative recognition and identification of hydrolocation fields produced by bodies of complex geometric shapes

V S Davydov

1. Introduction

Observation of an underwater situation on the screen of a hydrolocation station (HLS) may reveal several targets simultaneously. The targets must therefore be recognized and identified for an appropriate decision to be taken.

Work on identifying bodies of complex shapes composed of individual structural elements whose size is several times larger than the wavelength of the wave irradiating them followed theoretical and experimental studies of the classification of information carried by hydrolocation fields reflected from bodies of simple geometric shapes (spheres, cylinders, etc.) and of the ability of dolphins to identify bodies of both simple and complicated shapes. In fact, a problem arose in creating automatic systems for identifying objects of complex shapes (this includes all real underwater objects in the sea, the sea bottom, and scuba divers) that would implement the dolphins' abilities. With this in mind, it was decided to use probe signals with a high resolution with respect to the distance between individual reflecting elements of bodies of complicated geometric shapes (short probe pulses whose spatial length is much shorter than the length of the target to be identified, long complex-shape probe pulses subsequently compressed in a correlated filter, or cross-correlation processing of hydrolocation signals with a copy of the probe pulse). Dolphins identify underwater objects by using short probe pulses. A detailed acoustic image can only be built at very short distances because of the limited size of hydroacoustic antennas. Arrival angles of reflected remote objects were measured with an accuracy of 10 to 15 degrees.

Uspekhi Fizicheskikh Nauk **178** (11) 1215 – 1235 (2008)
DOI: 10.3367/UFNr.0178.200811d.1215
Translated by V I Kisin, E G Strel'chenko, N A Raspopov; edited by A M Semikhatov

2. Multialternative recognition and identification of bodies of complex geometric shapes

The envelope of a reflected signal $S(t)$ (or the envelope of the cross-correlation function of hydrolocation signals with a copy of a complex-shape probe pulse) is a single-peak structure if probe pulses with a high resolution with respect to the distance to the reflecting elements are used. Significant maxima correspond to reflection from individual reflecting elements (Fig. 1). The envelope $S(t)$ displayed more than 30 attributes characterizing the structural and acoustic properties of the body to be identified. The most informative attributes had to be found.

In the present experimental study, algorithms were elaborated for identifying the attributes of $S(t)$, including the most complex algorithm for the identification of essential maxima, based on satisfying two relations for maximum maximorums and minimum minimorums [1]

$$\frac{S_j^{\max}}{S_{j-k}^{\min}} \geqslant \varDelta\,, \qquad \frac{S_j^{\max}}{S_{j+n}^{\min}} \geqslant \varDelta\,.$$

(The correctness and originality of these algorithms were verified by the St. Petersburg Division of the Steklov Mathematical Institute, RAS.)

Experimental physical hydroacoustic-pool modeling of hydrolocation fields of bodies of complex geometric shape has established that the amplitude components of significant maximums are extremely sensitive to changes in irradiation

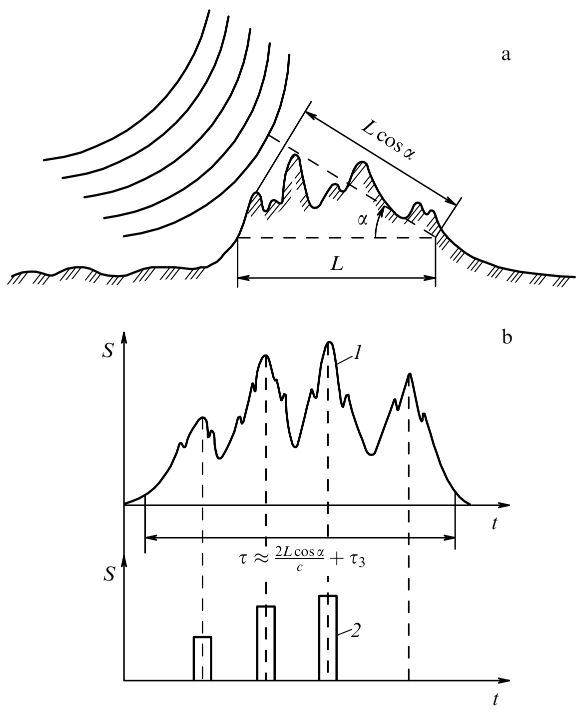

Figure 1. (a) Reflection of a short probe pulse from a body with a complex geometric shape. (b) Envelope of the echo signal reflected by a body with a complex geometric shape, of length L, obtained by using a short probe pulse of a length τ_ξ ($c\tau_\xi/2 \ll L$); *1*, experimental envelope; *2*, calculated envelope of the echo signal obtained when taking only its mirror component into account.

angles; histograms of the attribute spaces of amplitude values of the maximums of $\{S_j\}$ overlap to a great extent for different bodies of complex geometric shape. At the same time, the attribute spaces of the positions of maximums on the time coordinate $\{\tau_j\}$ are more stable relative to changes in the irradiation angle and differ greatly for different bodies of complex geometric shape in the range of locating angles of the order of 15°.

For an exact evaluation of the information content of the attributes, it was necessary to work out optimal decision rules for identifying hydrolocation signals from bodies of complex geometric shapes using multidimensional attribute spaces as a basis.

Physical studies showed that the distribution curves of the attributes $\{\tau_j\}$, $\{S_j\}$ and lengths τ of hydrolocation signals may generally have an arbitrary form, including a multimodal form. This statement was verified with experimental data by applying the nonparametric Kolmogorov – Smirnov agreement criterion [2]. Therefore, the approximation of conditional probability densities was satisfied. Because individual local maxima $S_j(t, \alpha, \beta)$ (where α and β are the angles at which the body is irradiated) in the envelope $S(t)$ are formed as a result of reflection of probe pulses from different reflecting elements with different directional characteristics, we can assume that fluctuations of positions in time $\{\tau_j\}$, the amplitude values $\{S_j\}$ of these maxima, and the time lengths τ are independent. This hypothesis was confirmed by testing the experimental data with the Spearman rank correlation criterion and the concordance coefficient [3]. The conditional multidimensional probability densities of the $\{\tau_j\}$, $\{S_j\}$, τ attribute spaces can be rewritten as the products

$$f\left(\bigcup_{j=1}^{n_i} \tau_j/A_i\right) = \prod_{j=1}^{n_i} f(\tau_j/A_i)\,,$$
$$f\left(\bigcup_{j=1}^{n_i} \hat{S}_j/A_i\right) = \prod_{j=1}^{n_i} f(\hat{S}_j/A_i)\,, \qquad (1)$$
$$f\left(\bigcup_{j=1}^{n_i} \tau_j\,,\, \tau/A_i\right) = \prod_{j=1}^{n_i} f(\tau_j/A_i)\, f(\tau/A_i)\,.$$

This transformation greatly simplified the construction of optimal decision rules. However, the dimension of attribute spaces changed continuously depending on the irradiation angles. In general, changes in the dimensions of the $\{\tau_j\}$, $\{S_j\}$ attribute spaces were calculated in the learning process by determining a priori probabilities of the formation and absence of significant maxima in certain local areas and by taking them into account in the process of recognition and identification. (The correctness and originality of this solution was confirmed by the St. Petersburg Division of the Steklov Mathematical Institute, RAS.) The rules of multialternative recognition of hydrolocation signals based on the multidimensional $\{\tau_j\}$, $\{S_j\}$ attribute spaces and the attribute τ were formulated in correspondence with the maximum likelihood criterion. These rules can be easily transformed to the Bayes criterion if the a priori probabilities of the presence of the bodies to be recognized are known and loss functions for mistaken recognition are known. For a one-dimensional attribute, the signal length τ, with the approximation of conditional one-dimensional probability densities taken into account using the Parsen – Rosenblatt method, the rule is given by

$$\sup_i \{\varphi_i\} = \sup_i \left\{ \frac{1}{N_i N_i^{-1/4}} \sum_{k=1}^{N_i} \frac{1}{\sigma\sqrt{2\pi}} \exp \frac{-1}{2\sigma^2} \left(\frac{\tau - \tau_{ki}}{N_i^{-1/4}} \right)^2 \right\}, \qquad (2)$$

where τ is the length of the measured echo signal, τ_{ki} are the sampled values of the lengths of the echo signals measured in the ranges $\Delta\alpha$ and $\Delta\beta$, N_i is the number of terms in the learning sample for the ith body, and σ is the rms deviation of lengths τ of the echo signals.

In the recognition following rule (2), the length τ of the echo signal and irradiation angles α_r and β_r for i bodies are measured, the sampled values τ_{ki} of attributes are taken in correspondence with the range of irradiation angles $\Delta\alpha$ and $\Delta\beta$ that contains α_r and β_r, the likelihood functions φ_i are calculated, and a decision is made on assigning the measured attribute τ to the ith body, if φ_i is the largest of all the φ_i, $i = 1, \ldots, M$.

The optimal decision rule for identifying and recognizing an object based on multidimensional attribute spaces of temporal positions of maximums of echo signals $\{\tau_j\}$ based on the maximum likelihood criterion is formed using master curves built as conditional probability densities in the angle irradiation range $\Delta\alpha$ and $\Delta\beta$ with the dimensions of the attribute spaces taken into account as a priori probabilities of finding (k_{ji}) and not finding ($1 - k_{ji}$) the values of the attributes in the jth reference areas for i bodies [4, 5]:

$$\sup_i \{\varphi_i\} = \sup_i \left\{ \prod_{j=1}^{m} k_{ji} f(\tau_j/A_i) \prod_{j=m+1}^{n_i} (1 - k_{ji}) \right\}, \qquad (3)$$

where m is the number of maxima in the measured echo signals whose temporal positions $\{\tau_j\}$ fall within the jth reference area of the ith body, n_i is the number of the jth reference area of the ith body, and $n_i - m$ is the number of reference areas of the ith body that did not receive the temporal positions of maximums $\{\tau_j\}$ in the measured echo signal.

With the approximation of conditional one-dimensional probability densities based on the Parsen–Rosenblatt method, decision rule (3) takes the form [4, 5]

$$\sup_i \{\varphi_i\} = \sup_i \left\{ \prod_{j=1}^{m} k_{ji} \frac{1}{N_{ji} N_{ji}^{-1/4}} \sum_{k=1}^{N_{ji}} \frac{1}{\sigma_\tau \sqrt{2\pi}} \times \exp \frac{-1}{2\sigma_\tau^2} \left(\frac{\tau_j - \tau_{jik}}{N_{ji}^{-1/4}} \right)^2 \prod_{j=m+1}^{n_i} (1 - k_{ji}) \right\}, \qquad (4)$$

where τ_j is the number of maximums in the envelope of the measured echo signals, τ_{jik} are the sampled values of temporal positions of maximums for the jth reference position of the ith body corresponding to the range of irradiation angles $\Delta\alpha$ and $\Delta\beta$, N_{ji} is the number of sampled values of τ_{jik} for the jth reference position of the ith body, and σ_τ is the rms deviation for the $\{\tau_j\}$ attribute space.

Before identification according to rule (4), or using attribute τ, it is necessary to measure the irradiation angles α_r and β_r and sample values of attributes τ_{jik} for the angle ranges $\Delta\alpha$ and $\Delta\beta$ that contain α_r and β_r. The decision whether the τ_j attribute space selected from the measured echo signal belongs to the ith body is taken according to the maximum value of the likelihood function φ_i among all the φ_i, $i = 1, \ldots, M$. Figure 2 gives an example of a three-alternative identification of bodies based on temporal positions of maximums in the envelopes of echo signals $\{\tau_j\}$. Reference attribute spaces $\{\tau_j\}$ for a 15° range of irradiation angles are given as conditional probability densities with the a priori probabilities $k_{ji} f(\tau/A_i)$ of finding attributes in the jth areas taken into account. Given below are the results of measurements of temporal positions of maximums $\{\tau_j\}$ in the echo signal. The values of likelihood functions φ_1, φ_2, and φ_3 were calculated for three bodies on the basis of these data. The highest value is reached by φ_1, and therefore the result of the identification is the decision that the measurement data $\{\tau_j\}$ belong to body 1.

The optimal rule for identifying bodies using normalized amplitude ratios of the maximums in the envelopes of echo signals $\{\hat{S}_j\}$ is formed, just as rule (4), by using their reference signals as conditional probability densities and with the a priori probabilities of finding (k_{ji}) and of not finding $(1 - k_{ji})$ the attributes in certain reference areas calculated on the basis of the $\{\tau_j\}$ attribute spaces.

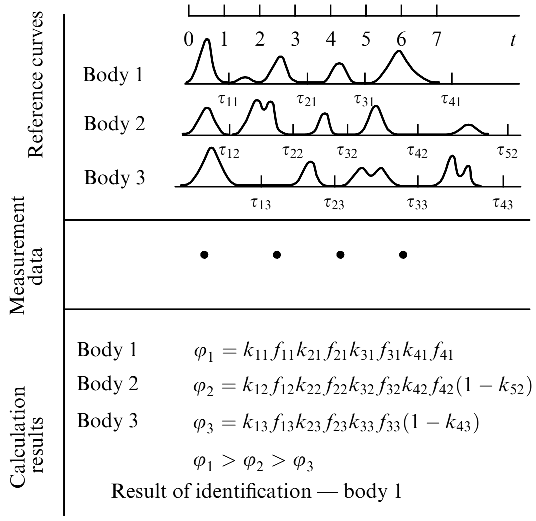

Figure 2. An example of the three-alternative identification of bodies of complex geometric shapes based on the attribute space of temporal positions of maximums on the envelopes of hydrolocation signals using the optimal decision rule.

Using the property of joint independence of the attributes $\{\tau_j\}$, $\{\hat{S}_j\}$ and $\{\tau_j\}$, τ, by analogy with the above procedures, we can construct the decision rules for jointly using these attributes [4]:

$$\sup_i \{\varphi_i\} = \sup_i \left\{ \prod_{j=1}^{m} k_{ji} f(\tau_j/A_i) f(\tau/A_i) \prod_{j=m+1}^{n_j} (1 - k_{ji}) \right\},$$
$$\sup_i \{\varphi_i\} = \sup_i \left\{ \prod_{j=1}^{m} k_{ji} f(\tau_j/A_i) f(\hat{S}_j/A_i) \prod_{j=m+1}^{n_j} (1 - k_{ji}) \right\}. \qquad (5)$$

Computer algorithms and software have been written for identifying bodies on the basis of attributes $\{\tau_j\}$, $\{\hat{S}_j\}$, and τ. The results of alternative identification of four bodies of complex geometric shapes for the range of irradiation angles of 10 to 15° are given in Table 1.

The highest probability of correct identification of bodies was obtained by using the $\{\tau_j\}$ attribute space [4, 5]. This therefore confirms the maximum information content of the attribute space of temporal positions of maxima in the envelopes of echo signals, $\{\tau_j\}$, dictated by the relative positions of reflectors on bodies of complex geometric

Table 1. The results of a separate identification of 1:100 scale models based on the attributes $\{\tau_j\}$, $\{S_j\}$, τ.

Frequency, kHz	Model number	Range of location angles, deg	Probability of correct identification using the optimal decision rule, %		
			based on $\{\tau_j\}$	based on $\{S_j\}$	based on τ
100	1, 2, 3, 5	5–20	89 (85–93)	55 (47–63)	65 (57–73)
1000	1, 2, 3	5–20	67 (57–77)		
350	1, 2, 3, 4	5–20	92 (87–97)	57 (47–67)	75 (65–85)
350	1, 2, 3, 4	22–38	79 (69–88)	39 (29–49)	40 (30–50)
350	1, 2, 3, 4	45–60	86 (79–92)	43 (33–53)	50 (40–60)
350	1, 2, 3, 4	60–75	76 (66–84)	43 (33–53)	32 (22–44)
350	1, 2, 3	105–120	76 (66–84)	48 (38–58)	24 (15–34)
350	1, 2, 3	135–150	95 (90–99)	62 (52–72)	62 (52–72)
350	1, 2, 3	160–175	100 (96–100)	76 (66–84)	71 (61–80)

shapes, in comparison with attributes related directly to the amplitude values of envelopes of echo signals. Appending the attributes $\{\hat{S}_j\}$ and τ to the attribute space $\{\tau_j\}$ increases the correct identification probability only insignificantly (by 3–5%). Identification on the basis of the $\{\tau_j\}$ but without taking the a priori probabilities k_{ji} of finding attributes in the jth reference areas into account reduced the probability of the correct identification of objects.

3. Method of analyzing reference signals

In using probe pulses with a high resolution with respect to the distance between reflecting elements, the level of the reflected signal $S(t)$ is somewhat lower than in the case of a long probe package covering the entire object to be recognized. For real objects, this difference amounts to 8–12 dB. Identification of bodies of complex geometric shapes in the sea meets with additional difficulties because of multipath propagation of signals in maritime conditions (this can sometimes be eliminated by adapting identification rules). A new principle of formation of hydrolocation signals was therefore suggested and a method of sending reference signals was developed resulting in incorporating the information on the targeted body of complex shape, in the form of the $\{\tau_j\}$ attribute space, into the probe signal.

To increase the noise immunity of the identification of bodies of complex shape from the effects of high-intensity noise and reverberation interference, it is suggested to form a reference probe signal as a sum of short pulses $\xi_k(t)$ [or long complex-shape probe pulses $\xi_c(t)$] such that the delays between them correspond to the reference values, arranged in reverse order, of the mutual positions of maximums $\{\tau_j\}$ on the echo signals of the identified body in a certain range of irradiation angles [4, 6]. The reference values for each jth maximum are then determined as mean values of the τ_j for all τ_j found at the learning stage in the jth region in the angular ranges $\Delta\alpha$ and $\Delta\beta$. Figure 3a shows an example of the envelope of the reflected signal $S(t)$ from a body of complex shape when using a short probe pulse $\xi_k(t)$ as the envelope of the generated reference signal $S_2(t)$, with delays $\{\tau_v\}$ between pulses with amplitudes a_v (assumed to be equal); envelopes of the signals $S_3(t)$, $S_4(t)$, and $S_5(t)$ reflected from each of the three elements of the body and the envelope of the total signal $S_\Sigma(t)$ reflected by the body as a whole are plotted only schematically. Representing the transmission function for a body of complex shape as a series of delta functions with delays $\{\tau_j\}$ and amplitudes a_j,

$$\varphi(t) = \sum_{j=1}^{n} a_j \delta(t - \tau_j)\,,$$

we can write the echo signal as a convolution

$$\begin{aligned} S_\Sigma(t) &= \int_{-\infty}^{\infty} S_2(t)\,\varphi(t-\tau)\,\mathrm{d}\tau \\ &= \int_{-\infty}^{\infty} S_2(t) \sum_{j=1}^{n} a_j \delta(t - \tau_j - \tau)\,\mathrm{d}\tau \\ &= \int_{-\infty}^{\infty} \sum_{v=1}^{n} a_v \xi(t)\,\varphi(t+\tau_v) \sum_{j=1}^{n} a_j \delta(t-\tau_j-\tau)\,\mathrm{d}\tau \\ &= \sum_{v=1}^{n}\sum_{j=1}^{n} a_v a_j \xi(t+\tau_v-\tau_j)\,. \end{aligned}$$

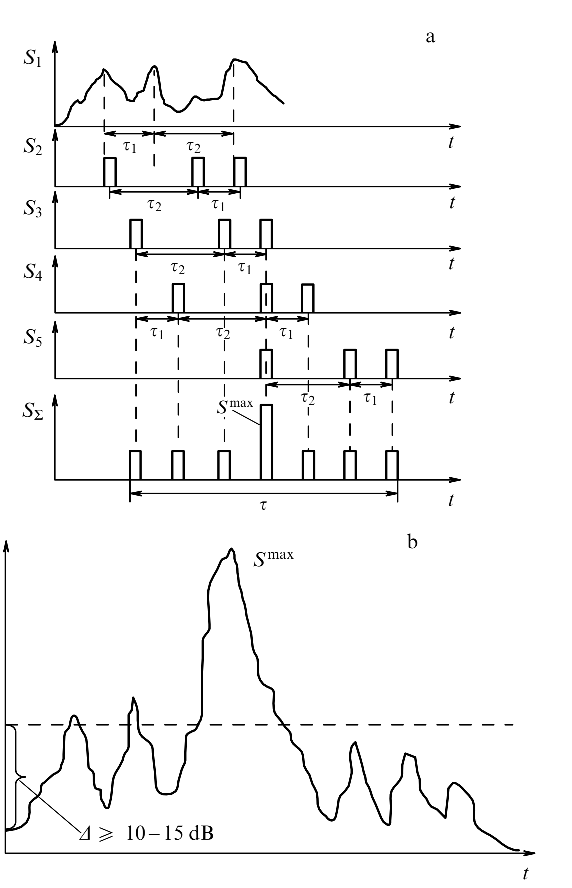

Figure 3. (a) A schematic representation of the formation of a global maximum $S^{\max}$ in the total signal $S_\Sigma(t)$ obtained by summing the reflections of the sent signal $S_2(t)$ from all three reflectors of a body of complex shape; $S_3(t)$, $S_4(t)$, and $S_5(t)$ are the respective signals reflected by the first, second, and third reflectors. (b) An example of a resulting global maximum $S^{\max}$ in $S_\Sigma(t)$.

If $\{\tau_j\}$ and $\{\tau_v\}$ coincide, then the signal $S_\Sigma(t)$ is equal to the sum of all reflected signals from all elements of the body. The shape of $S_\Sigma(t)$ displays a global maximum $S_\Sigma^{\max}$ greater than the average level of the envelope $\bar{S}_\Sigma(t)$ [4, 6]. If $S_2(t)$ is formed as a sum of long complex-shape probe pulses $\xi_c(t)$, then a short $S_\Sigma^{\max}$ is observed after correlated filtration and detection of $S_\Sigma(t)$. Identification of a complex-shape body is carried out, for instance, when the ratio $S_\Sigma^{\max}/\bar{S}_\Sigma$ exceeds the threshold level. In this way, it is possible to identify a complex-shape body for which the reference values $\{\tau_j\}$, its identification against the background of signals from other complex-shape bodies, or the reverberation or noise interference is known.

Figure 3b gives an example of the envelope $S_\Sigma(t)$ [in the case of using $\xi_k(t)$] after sending $S_2(t)$. Identification of a body of complex shape is then carried out for $S_\Sigma^{\max}/\bar{S}_\Sigma > \psi$, in which case the noise level may be comparable with $\bar{S}_\Sigma$, that is, the noise immunity increases by Δ [dB] relative to the noise immunity with identification methods using only one probe pulse.

This method of sending reference signals was investigated in model hydrolocation measurements in a hydroacoustic tank.

The curves $S^{\max}/\bar{S}_\Sigma$ and $S^{\max}/\bar{S}_{\Sigma_{1/3}}$ were plotted (where $\bar{S}_{\Sigma_{1/3}}$ indicates that the mean value of the signal was measured at 1/3 of the length of $S_\Sigma(t)$ before $S^{\max}$ was

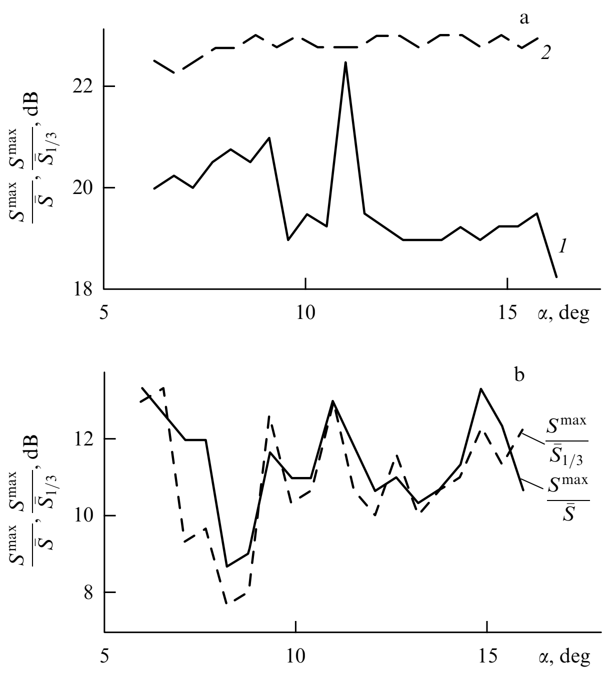

Figure 4. (a) The ratio of the amplitudes of global maximums $S^{\max}$ to the average levels of the envelopes $S(t)$ as a function of the irradiation angle α in response to irradiation by a reference signal: *1*, $S^{\max}/\bar{S}$ as a function of α; *2*, $S^{\max}/\bar{S}_{1/3}$ as a function of α. (b) The ratio of the amplitudes of global maximums $S^{\max}$ to the average levels of the envelopes $S(t)$ as a function of the irradiation angle α in response to irradiation by a train of seven equidistant pulses.

formed). Figure 4a gives an example of this dependence on the irradiation angle for a body in the horizontal plane, $\alpha = 5-15°$; the reference signal was formed in the irradiation of the body at $\alpha_0 = 10°$. Figure 4b gives an example of these curves for irradiation of the same body with seven equidistant pulses [the number of maximums in $S_\Sigma(t)$ is also roughly equal to 7]. These curves were plotted for probe pulses of equal length and for equal ranges of the body irradiation angle. On average, the ratios $S^{\max}/\bar{S}_{\Sigma_{1/3}}$ were greater than $S^{\max}/\bar{S}_\Sigma$, but the difference was insignificant. A comparison of the plots shown in Figs 4a and b demonstrates that the ratios $S^{\max}/\bar{S}_\Sigma$ and $S^{\max}/\bar{S}_{\Sigma_{1/3}}$ obtained for irradiation by reference signals at all angles were greater than the values in the case of equidistant pulses, which corresponds to irradiating a body with an extraneous reference signal. In this case, correct identification was faultless at all irradiation angles.

With this approach, the problem of identification is greatly simplified and in fact reduces to the problem of locating the global maximum. The price paid for increasing the noise immunity under multialternative identification is the need to send several reference signals whose number equals that of the bodies to be recognized. If reference signals are sent, the total information on the distribution of reference values $\{\tau_j\}$, incorporated in the conditional probability densities $f(\bigcup_{i=1} \tau_j)$, is not used. However, identification can be achieved by using the optimal criterion.

The suggested method is most convenient for identification of a known body against a background of noise and reverberation interference and in identifying complex-shape bodies in a multipath environment. Multipath propagation of signals in marine environments produces not one but several maxima $S_\Sigma^{\max}$ on $S_\Sigma(t)$ (depending on the hydrological environment). However, the procedure for identifying complex-shape bodies does not change in this case.

References

1. Davydov V S "Algoritm vyyavleniya sushchestvennykh maksimumov v ogibayushchei signala" ("Algorithm of identifying significant maximums on the signal envelope"), in *Modeli, Algoritmy, Prinyatie Reshenii*: *Tezisy 2-go Vsesoyuz. Akusticheskogo Seminara* (*10–14 Okt. 1988, Leningrad*) (Models, Algorithms, Decision Making: Abstracts of 2nd USSR Acoustic Seminar (Oct. 10–14, 1988, Leningrad)) (Moscow: N.N. Andreev Acoustic Inst., USSR Acad. Sciences, 1988) p. 65
2. Bondar L F, Davydov V S "Issledovanie funktsii raspredeleniya priznakov, primenyaemykh dlya raspoznavaniya podvodnykh skal i donnykh gruntov" ("Distribution functions of attributes used for identifying underwater rocks and bottom soil"), in *Trudy 9-i Vsesoyuz. Konf. po Informatsionnoi Akustike* (*Mart 1985 g.*) (Proc. of the 9th USSR Conf. on Information Acoustics (March 1985)) (Moscow: N.N. Andreev Acoustic Inst., USSR Acad. Sciences, 1987) p. 98
3. Davydov V S "Issledovanie statisticheskikh svoistv impul'snukh posledovatel'nostei, obuslovlennykh gruppoi zhestko svyazannykh otrazhatelei" ("Statistical properties of pulse sequences prepared for a group of rigidly connected reflectors), in *Obrabotka Akusticheskoi Informatsii v Mnogokanal'nykh Sistemakh* (Processing of Acoustic Information in Multichannel Systems) Issue 15 (Ed. V V Rotin) (Leningrad: Sudostroenie, 1988) p. 41
4. Davydov V S *Raspoznavanie v Gidrolokatsii* (Identification and Recognition in Hydrolocation) (St.-Petersburg: SPbGTEU 'LETI', 2005)
5. Davydov V S "Optimal'noe reshayushchee pravilo dlya raspoznavaniya tel slozhnoi geometricheskoi formy po otrazhennym gidroakusticheskim signalam" ("Optimum decision rule for identification of bodies of complex geometric shapes using reflected hydroacoustic signals"), in *Chelovek i Okean*: *Trudy Dokladov IV Dalnevostochnoi Konf. "Akusticheskie Metody i Sredstva Issledovaniya Okeana* (Man and the Ocean: Proc. of the IVth Far East Conf. "Acoustic Methods and Techniques for Ocean Research) (Vladivostok: AN SSSR, Far Eastern Research Center, 1986) p. 32
6. Davydov V S "Povyshenie pomekhozashchishchennosti raspoznavaniya tel slozhnoi formy po otrazhennym akusticheskim signalam" ("Increasing noise immunity of identification of bodies of complex shapes by using reflected acoustic signals") *Tekh. Akust.* **3** (1–2 (7–8)) 59 (1994)

PACS numbers: **12.20.–m**, 12.20.Ds, 31.30.Gs, 31.30.Jv
DOI: 10.1070/PU2008v051n11ABEH006801

Quantum electrodynamics of heavy ions and atoms: current status and prospects

V M Shabaev

1. Introduction

Quantum electrodynamics (QED), whose underlying principles were formulated by Dirac, Heisenberg, Born, Fock, Pauli, Wigner, Jordan, Fermi, and others by the early 1930s, has been quite successful in describing the emission (absorption) of a photon by an atom and the creation (annihilation) of electron–positron pairs, but second-order perturbative QED calculations yielded infinite results for some effects. This problem remained unsolved until about the late 1940s, when experiments by Lamb and Rutherford revealed what is now known as the Lamb shift, the splitting of the 2s and $2p_{1/2}$ energy levels in the hydrogen atom. Because there was virtually no doubt about the quantum-electrodynamic origin of the Lamb shift, this discovery paved the way to the solution to the problem of singularities. The Lamb shift was first estimated by Bethe, and the modern theory of quantum electrodynamics, which solved the problem of infinities via the renormalization procedure, was developed by Dyson, Feynman, Tomonaga, and Schwinger. Because of the presence of a small parameter (the fine structure constant $\alpha \approx 1/137$), QED calculations rely on the perturbation theory, in which the Feynman diagram representation of each term enables formulating simple rules for writing formal mathematical expressions.

Until about the early 1980s, the only atoms that allowed testing QED were light ones such as hydrogen, positronium, helium, and muonium. For these, in addition to α, there is a small parameter αZ, where Z is the nucleus charge. For this reason, QED calculations for light atoms were limited to the few lowest orders in α and αZ, and comparison of theory and experiment only allowed testing the QED in the lowest orders in these parameters. This being a rather narrow testing range, the question naturally arises as to how to extend it. The immediate answer seems to be to go to higher orders in αZ to investigate QED effects for inner electrons in heavy neutral atoms (for example, the uranium atom), which are known to be in a strong (nonscreened) Coulomb field of the nucleus and for which the parameter αZ is not small. But the uncertainty in correlation effects, which usually is at or even exceeds the level of QED contributions, places strong accuracy constraints on the theoretical calculation of such systems. For this reason, heavy neutral atoms are usually treated only by means of the Breit equation, in which relativistic correlation effects are taken into account only approximately. The unique possibility of testing QED to all orders in terms of αZ has occurred with the advent of high-precision experiments on heavy multiply charged ions (such as hydrogen-like [1] or lithium-like [2–4] uranium ions) in which, on the one hand, αZ is not small (in uranium, $\alpha Z \approx 0.7$) and, on the other hand, because of the small number of electrons, correlation effects (i.e., electron–electron interaction effects) can be calculated to a high accuracy. It is the theory of such systems that occupies the bulk of this talk. As regards heavy neutral atoms, our discussion is brief and limited to recent advances in calculating QED corrections to spatial parity violation effects in neutral cesium (these corrections are very important for testing the Standard Model (SM) at low energies).

Relativistic units $\hbar = c = 1$ are used throughout the talk.

2. Binding energies of heavy ions

Because the number of electrons in a multiply charged ion is much smaller than the nucleus charge Z and because, therefore, the electrons interact much more strongly with the nucleus than with one another, a reasonable first approximation is that they do not interact at all and obey the one-electron Dirac equation in the Coulomb field $V_{\mathrm{C}}(r)$ of the nucleus,

$$\big(\boldsymbol{\alpha}\mathbf{p} + \beta m + V_{\mathrm{C}}(r)\big)\psi(\mathbf{r}) = E\psi(\mathbf{r})\,. \tag{1}$$

For a point-like nucleus, the Dirac equation is solved analytically. For a finite-size nucleus, both numerical and analytic solutions can be obtained [5].

QED corrections and those for the electron–electron interaction are included perturbatively. The corrections for the electron–electron interaction are suppressed by the parameter $1/Z$, which for heavy ions is comparable to the QED correction parameter α. Therefore, in the case of heavy ions, all the contributions are more conveniently characterized by the single parameter α. We note that unlike for light atoms, calculations for heavy atoms should be carried out without expanding in αZ.

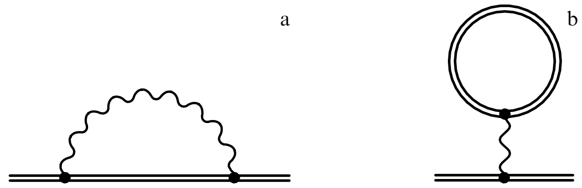

Figure 1. First-order one-electron diagrams: self-energy and vacuum polarization.

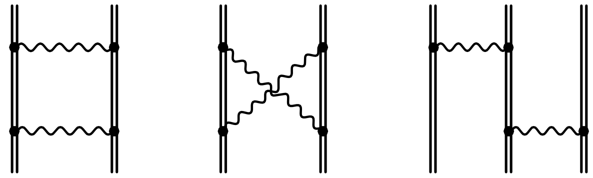

Figure 2. Two-photon exchange diagrams.

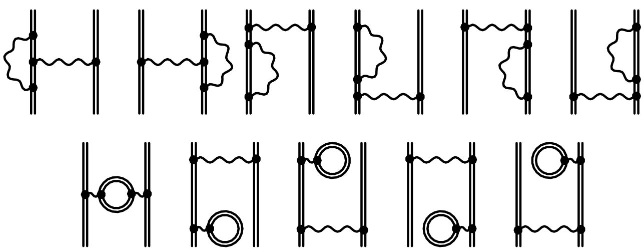

Figure 3. Screened-self-energy and vacuum polarization diagrams.

Because the electron mass is much smaller than the mass of the nucleus, most contributions can be calculated in the approximation of an infinitely heavy nucleus, when the nucleus simply serves as a source of an external Coulomb field and we are dealing with quantum electrodynamics in the Furry picture. First-order calculations in α should be done for contributions from the self-energy (Fig. 1a) and vacuum polarization (Fig. 1b) diagrams. For ions with two or more electrons, the one-phonon exchange diagram should of course also be included, and is rather easy to calculate. The main technical problem with calculating the self-energy and vacuum polarization diagrams is working without expanding in αZ. The first such calculations were performed in Ref. [6] for the self-energy diagram and in Refs [7, 8] for the vacuum polarization diagram.

The next stage in performing calculations in the Furry picture is to evaluate the contributions from second-order two- and three-electron diagrams, which include two-photon exchange diagrams (Fig. 2), as well as screened self-energy and vacuum polarization diagrams (Fig. 3). For this, the first thing to do is to derive the necessary calculation formulas. This problem mainly refers to the so-called reducible diagrams, i.e., those in which the total energy of an intermediate state of the atom equals the unperturbed energy of the reference state; for the remaining (irreducible) diagrams, the derivation poses no difficulty. In the late 1980s,

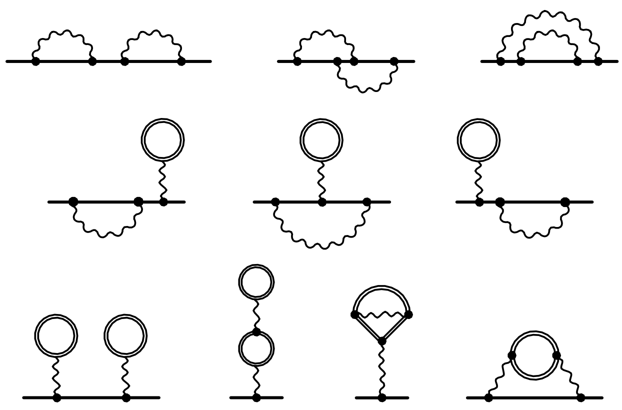

Figure 4. Second-order one-electron diagrams.

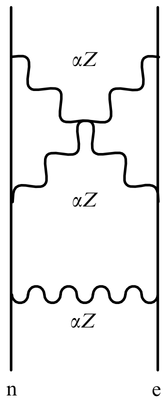

Figure 5. Typical diagram for the electron – nucleus interaction.

when the calculation of these diagrams was of particular topical interest, it was found that the adiabatic S-matrix formalism of Gell-Mann and Low, the most common approach at the time, has a number of drawbacks that make it computationally impractical. These include, among others, prohibitive technical difficulties in treating reducible diagrams, the lack of the renormalizability proof, the impossibility to calculate the energies of quasidegenerate states, and the unavailability of any analogous method capable of calculating transition amplitudes. All of these problems were overcome by using the method of two-time Green's functions developed for this purpose in Ref. [9] (see Ref. [10] for a detailed description). In particular, this method has been used to solve, for the first time, the computationally most challenging problem of deriving an expression for two-electron two-photon exchange diagrams [9]. In Ref. [11], this expression was calculated numerically for the ground state of helium-like atoms without expanding in αZ. Screened self-energy and vacuum polarization diagrams were calculated in Refs [12 – 14], followed by calculations for lithium-like ions [15] and for the excited states of helium-like atoms [16]. Recently, the full set of diagrams shown in Figs 2 and 3 were finally calculated for the $2p_{3/2} - 2p_{1/2}$ transition for the boron-like argon ion [17].

Referring to the second-order one-electron diagrams in Fig. 4, calculations for some of these reduce to calculating first-order diagrams. An example is given by the diagrams shown in the second row of the figure, where the calculation reduces to the ordinary one-loop self-energy calculation for an effective potential composed of the Coulomb potential of the nucleus plus the vacuum polarization potential. At the same time, two-loop self-energy diagrams (seen in the first row of Fig. 4) pose challenging technical difficulties for calculation, as also do the last two diagrams in the figure. Considerable progress in this area was made in the relatively recent study in Refs [18, 19], where the full set of two-loop self-energy diagrams was calculated.

In these calculations, the nucleus is treated as an infinitely massive source of an external Coulomb field. Going beyond this approximation requires taking the finite mass of the nucleus, that is, the recoil effect, into account. In the nonrelativistic theory of a hydrogen-like atom, it is known that the recoil effect of the nucleus is readily taken into account by introducing the reduced electron mass $\mu = mM/(m+M)$. But this is not the case in the relativistic theory, which can only be formulated in the QED framework. A fully relativistic theory accounts for the nuclear recoil effect by considering all the diagrams for the electron – nucleus interaction via photon exchange. A typical example of such a diagram is shown in Fig. 5. The fact that each photon line in this diagram contributes a factor αZ explains the fundamental difference in how the theory accounts for the recoil effect in light and heavy atoms. For light (small-αZ) atoms, a calculation with only a few lowest-order diagrams is a sufficient approximation, but for heavy ions, in which the parameter αZ is not small, no finite number of diagrams suffice and, instead, the infinite sequence of such diagrams must be summed (at least in the first order in m/M). Because the standard QCD formalism offers no recipes for doing this, we are faced with a serious conceptual problem here. Reference [20] was the first to set out to derive a closed expression accurate to all orders in αZ for the nuclear recoil effect. The next important development in this area was the demonstration in Ref. [21] of the summability of the infinite sequences of diagrams of interest here. Full closed formulas for recoil corrections, accurate in the first order in m/M and exact in αZ, were obtained by the quasipotential method in Ref. [22]. According to these formulas, the recoil correction to the energy of the bound state a of a hydrogen-like atom is the sum of the lower and higher (in αZ) contributions,

$$\Delta E_{\mathrm{L}} = \frac{1}{2M} \langle a | \left[\mathbf{p}^2 - \left(\mathbf{D}(0)\,\mathbf{p} + \mathbf{p}\,\mathbf{D}(0) \right) \right] | a \rangle \,, \tag{2}$$

$$\Delta E_{\mathrm{H}} = \frac{\mathrm{i}}{2\pi M} \int_{-\infty}^{\infty} \mathrm{d}\omega \left\langle a \middle| \left(\mathbf{D}(\omega) - \frac{[\mathbf{p}, V_{\mathrm{C}}]}{\omega + \mathrm{i}0} \right) G(\omega + E_{\mathrm{a}}) \right.$$
$$\left. \times \left(\mathbf{D}(\omega) + \frac{[\mathbf{p}, V_{\mathrm{C}}]}{\omega + \mathrm{i}0} \right) \middle| a \right\rangle . \tag{3}$$

Here, $\mathbf{p}$ is the momentum operator, $G(\omega)$ is the relativistic Coulomb Green's function, $D_m(\omega) = -4\pi\alpha Z \alpha_l D_{lm}(\omega)$, and $D_{ik}(\omega, r)$ is the transverse part of the Coulomb gauge photon propagator. We note that the scalar product is understood in Eqn (3). Reference [23], also relying on the quasipotential method, extended these formulas to atoms with several electrons. In later studies [24], other methods were used to derive formulas (2) and (3). The first numerical calculations with these formulas were performed in Ref. [25].

It is necessary, finally, to account for the polarization of the nucleus by the electron. This effect is represented by the diagrams of the two-photon exchange between the nucleus and an electron in which intermediate (virtual) states of the

Table 1. Energy of the $2p_{1/2}-2s$ transition in the Li-like uranium ion.

	Energy, eV
Breit approximation	322.13(7)
QED contributions of the first order in α	-42.93
QED contributions of the second order in α	1.55(7)
Nuclear recoil	-0.07
Nuclear polarization	0.03(1)
Full theoretical value	280.71(10)
Experimental value [4]	280.645(15)

nucleus are excited. Given that the internucleon interaction is understood only phenomenologically, calculating nuclear polarization is a serious physical problem, and it is in fact the errors from this calculation that determine the upper-bound accuracy of the full theoretical values needed. Calculations of this effect for heavy hydrogen-like ions were carried out in Refs [26, 27].

To date, the highest level of precision has been achieved in experiments to measure transition energies in lithium-like ions [2–4]. Table 1 shows the values of different contributions to the $2p_{1/2}-2s$ transition energy and compares the full theoretical value with the experimental result. The contribution due to the finite size of the nucleus is calculated for a Fermi nuclear charge distribution with account for the nuclear deformation [28]. It is seen that as far as lithium-like uranium is concerned, the current theory and experiment provide about a 0.2% test of QED in a strong Coulomb field.

3. Hyperfine structure

A number of high-precision measurements are available for determining the hyperfine ground state splitting of heavy hydrogen-like ions [29–32]. The primary motivation behind these measurements was the fact that in a heavy ion with nonzero nuclear spin, each electron experiences, in addition to the strong Coulomb field, a very strong magnetic field created by the magnetic moment of the nucleus; this a situation provides a unique opportunity for testing QED in the combination of the highest currently achievable electric and magnetic fields. The first such experiment was carried out on bismuth [29] and yielded the value 5.0840(8) eV for the hyperfine ground state splitting of the H-like ion $^{209}Bi^{82+}$. The theoretical value of the hyperfine splitting is conveniently written as

$$\Delta E = \Delta E_{\rm Dirac}(1-\varepsilon) + \Delta E_{\rm QED}\,, \tag{4}$$

where the Dirac value includes relativistic effects and the nuclear charge distribution correction, ε is the (Bohr–Weisskopf) correction for the nuclear magnetic moment distribution, and $\Delta E_{\rm QED}$ is the QED correction. Calculating $\Delta E_{\rm Dirac}$ is straightforward. The QED correction has also been calculated by several groups, leading to reasonably consistent results. The main problem consists in calculating the Bohr–Weisskopf correction, which, because of its high sensitivity to the nuclear model, almost entirely determines the full theoretical uncertainty. For the H-like ion of bismuth, a calculation within a one-particle model of the nucleus yields the hyperfine splitting 5.101(27) eV [33], a value that agrees with experiment but contains a large error. A more accurate calculation for a many-particle nuclear model [34] yields $5.111(-3,+20)$ eV, which is in disagreement with experiment. Finally, a semiempirical calculation using an experimental value of hyperfine splitting in muonic bismuth yielded 5.098(7) eV [35], about two standard deviations from the experimental value. The QED contribution to the given hyperfine splitting is about -0.030 eV and is in fact comparable to the error in the Bohr–Weisskopf correction. Although this fact prevents the tests of QED by directly comparing theoretical and experimental results for the hyperfine structure of hydrogen-like ions, it has been shown [36] that QED effects can be experimentally identified by using a certain particular difference between the hyperfine splitting of H- and Li-like ions of the same isotope,

$$\Delta' E = \Delta E^{(2s)} - \xi \Delta E^{(1s)}\,, \tag{5}$$

where ξ is chosen so as to cancel the Bohr–Weisskopf effect. It turns out that both the parameter ξ and the difference $\Delta' E$ itself are weakly sensitive to variations in the nuclear model and can therefore be calculated to high precision. With this approach, it will be possible to test QED at the level of a few percent if the hyperfine splittings are measured to an accuracy $\sim 10^{-6}$. Such experiments are currently underway in Germany and the UK in the framework of the HITRAP (Heavy Ion Trap) project. The first experimental data on the hyperfine splitting in Li-like bismuth were obtained at the Livermore National Laboratory in the USA.

4. *g*-factor of multicharged ions

Precision *g*-factor measurements of the H-like carbon ion in a Penning trap [37] have generated considerable interest in the calculation of this quantity. The measurements were so accurate that their total precision was mainly determined by uncertainties in the electron mass m, which enters the formula for the *g*-factor along with the experimentally measured cyclotron and Larmor frequencies. This implies that knowing the theoretical value of the *g*-factor to within the desired accuracy would enable the electron mass to be determined with an accuracy exceeding that of the then-accepted value of m by several times. At the time, the two factors that determined the error in the theoretical value were the non-calculated higher-order nuclear recoil contributions and the error from the numerical calculation of the one-loop self-energy. Efforts to reduce the former resulted in a closed relativistic formula for the nuclear recoil correction to the atomic *g*-factor. Specifically, the following formula was derived, in the first order in m/M and in all orders in αZ, for the contribution from the nuclear recoil effect to the *g*-factor of an H-like ion [38]:

$$\Delta g = \frac{1}{\mu_0 m_{\rm a}} \frac{\rm i}{2\pi M} \int_{-\infty}^{\infty} {\rm d}\omega \left[\frac{\partial}{\partial B} \langle a | [\mathbf{p} - \mathbf{D}(\omega) + e\mathbf{A}_{\rm cl}] \times G(\omega + E_{\rm a}) [\mathbf{p} - \mathbf{D}(\omega) + e\mathbf{A}_{\rm cl}] | a \rangle \right]_{B=0}. \tag{6}$$

Here, μ_0 is the Bohr magneton, $m_{\rm a}$ is the projection of the moment on the z axis, $e = -|e|$ is the electron charge, and $\mathbf{A}_{\rm cl} = [\mathbf{B} \times \mathbf{r}]/2$ is the vector potential of the homogeneous magnetic field $\mathbf{B}$ directed along the z axis. It is assumed that all quantities are calculated in the presence of a magnetic field. A numerical calculation using expression (6) was carried out in Ref. [39], and a calculation of the one-loop self-energy to the required accuracy was performed in Ref. [40]. All in all, the comparison of the theoretical and experimental values of the *g*-factor of H-like carbon reduced the error in the value of the electron mass by a factor of four. These results, along with relevant studies on H-like oxygen [41], formed the basis for a new value of m as given in the most recent compilation of fundamental constants [42].

It is expected that the g-factors of multicharged ions up to $Z = 92$ can be experimentally determined in the very near future in the framework of the HITRAP project. For ions with nonzero spin, such experiments can be used to determine nuclear magnetic moments to within $\sim 10^{-6}$. As shown in Ref. [43], the fine structure constant can also be independently measured in this way.

5. QED corrections to the parity-violating 6s – 7s amplitude in neutral Cs

The study of parity violation remains one of the major tools for testing the Standard Model electroweak sector at low energies [44]. The measurement of the parity-violating 6s – 7s amplitude in neutral Cs to within 0.3% [45] required for both calculating new corrections to this amplitude and revising those contributions already calculated. As a result, more accurately accounting for correlation effects [46], combined with the Breit interaction [47, 48] and vacuum polarization [49] corrections, has led to a weak charge of the cesium ion, differing by 2σ from the SM prediction. It became clear that testing the SM requires a consistent QED calculation of self-energy corrections. The first estimates of this effect were made for the so-called 'mixing coefficients' of the s and p states, the coefficients being rather artificial entities in the QED context. Although both references gave similar results for the total (minus $-\alpha/2\pi$) binding QED correction [$-0.5(1)\%$ in Ref. [50] and $-0.43(4)\%$ in Ref. [51]), only a calculation of the total gauge-invariant set of self-energy corrections to the P-violating amplitude could answer the question of agreement or disagreement with the Standard Model. Such a calculation was carried out is Ref. [52], where it was assumed that a valence electron moves in an effective local potential constructed from the nonlocal Dirac – Fock potential. The result for the total binding QED correction was $-0.27(3)\%$, differing by a factor of two from previous estimates. Later, a similar result was obtained in Ref. [53], where a revision of the previous calculations in Refs [50, 51] was performed.

Combining the QED contribution with other contributions and comparing the resulting total amplitude with the averaged experimental value of the vector polarizability $\beta = 26.99(5)a_{\mathrm{B}}^3$ (see Ref. [46] and the references therein), the weak charge of ^{133}Cs is found to be

$$Q_{\mathrm{W}} = -72.65(29)_{\mathrm{exp}}(36)_{\mathrm{th}}\,, \tag{7}$$

which is 1.1σ from the SM prediction $-73.19(13)$ [54].

6. Conclusion

In this paper, theoretical results of the quantum electrodynamics of multicharged ions are presented and compared with experimental data, identifying the study of transition energies in heavy multicharged ions as the area where the QED in strong electric fields has by now been most thoroughly tested. A study of how QED affects the hyperfine structure of heavy ions, which would mean testing QED in the simultaneous presence of strong electric and magnetic fields, is greatly complicated by large uncertainties in corrections due to the nuclear magnetic moment distribution. The considerable reduction in these uncertainties for a certain particular difference of hyperfine splittings in H- and Li-like ions raises hope that such testing will become possible when necessary experiments, both underway and planned, are completed. The high-precision measurements of the g-factors of multicharged ions and a corresponding theory that has been developed have already resulted in a more accurate value of the electron mass and are expected to be used in the very near future to test QED in an external magnetic field and to obtain high-precision values of nuclear magnetic moments. It can be expected that these studies will also enable an independent, high-precision determination of the fine structure constant in the near future.

Large errors in calculating correlation effects in heavy neutral atoms make these systems impractical for verifying QED. However, when particularly precise calculations are to be made (for example, in estimating parity violation in a neutral Cs atom), QED corrections should be included. Computational QED techniques that have been developed for multicharged ions with a few electrons proved to apply to such systems as well. From a theoretical standpoint, what currently limits the tests of the Standard Model in neutral atoms is errors in correlation effects. In this connection, the study of parity violation in multicharged ions [55], where the accuracy of calculation is not subject to such limitations, holds considerable promise.

This work was supported in part by the RFBR grant No. 07-02-00125 and by the INTAS-GSI grant No. 06-10000012-8881.

References

1. Gumberidze A et al. *Phys. Rev. Lett.* **94** 223001 (2005)
2. Schweppe J et al. *Phys. Rev. Lett.* **66** 1434 (1991)
3. Brandau C et al. *Phys. Rev. Lett.* **91** 073202 (2003)
4. Beiersdorfer P et al. *Phys. Rev. Lett.* **95** 233003 (2005)
5. Shabaev V M *J. Phys. B: At. Mol. Opt. Phys.* **26** 1103 (1993)
6. Mohr P J *Ann. Phys.* (New York) **88** 26 (1974)
7. Soff G, Mohr P J *Phys. Rev. A* **38** 5066 (1988)
8. Manakov N L, Nekipelov A V, Fainshtein A G *Zh. Eksp. Teor. Fiz.* **95** 1167 (1989) [*Sov. Phys. JETP* **68** 673 (1989)]
9. Shabaev V M *Teor. Mat. Fiz.* **82** 83 (1990) [*Theor. Math. Phys.* **82** 57 (1990)]; *Izv. Vyssh. Uchebn. Zaved. Ser. Fiz.* **33** (8) 43 (1990) [*Sov. Phys. J.* **33** 660 (1990)]
10. Shabaev V M *Phys. Rep.* **356** 119 (2002)
11. Blundell S A et al. *Phys. Rev. A* **48** 2615 (1993); Lindgren I et al. *Phys. Rev. A* **51** 1167 (1995)
12. Persson H et al. *Phys. Rev. Lett.* **76** 204 (1996)
13. Artemyev A N, Shabaev V M, Yerokhin V A *Phys. Rev. A* **56** 3529 (1997)
14. Yerokhin V A, Artemyev A N, Shabaev V M *Phys. Lett. A* **234** 361 (1997)
15. Artemyev A N et al. *Phys. Rev. A* **60** 45 (1999); Yerokhin V A et al. *Phys. Rev. A* **60** 3522 (1999); Yerokhin V A et al. *Phys. Rev. Lett.* **85** 4699 (2000); Sapirstein J, Cheng K T *Phys. Rev. A* **64** 022502 (2001); Andreev O Yu et al. *Phys. Rev. A* **67** 012503 (2003)
16. Artemyev A N et al. *Phys. Rev. A* **71** 062104 (2005)
17. Artemyev A N et al. *Phys. Rev. Lett.* **98** 173004 (2007)
18. Yerokhin V A, Indelicato P, Shabaev V M *Phys. Rev. Lett.* **91** 073001 (2003); *Zh. Eksp. Teor. Fiz.* **128** 322 (2005) [*JETP* **101** 280 (2005)]
19. Yerokhin V A, Indelicato P, Shabaev V M *Phys. Rev. Lett.* **97** 253004 (2006)
20. Labzovskii L N, in *Doklady 17-ogo Vsesoyuznogo Siezda po Spektroskopii, Minsk, 1971* (Proceedings of the 17th All-Union Congress on Spectroscopy, Minsk, 1971) Pt. 2 *Teoriya Atomnykh Spektrov* (Theory of Atomic Spectra) (Moscow, 1972) p. 89
21. Braun M A *Zh. Eksp. Teor. Fiz.* **64** 413 (1973) [*Sov. Phys. JETP* **37** 211 (1973)]
22. Shabaev V M *Teor. Mat. Fiz.* **63** 394 (1985) [*Theor. Math. Phys.* **63** 588 (1985)]
23. Shabaev V M *Yad. Fiz.* **47** 107 (1988) [*Sov. J. Nucl. Phys.* **47** 69 (1988)]

24. Yelkhovsky A S, Preprint No. 94-27 (Novosibirsk: Budker Inst. of Nucl. Phys., 1994); Pachucki K, Grotch H *Phys. Rev. A* **51** 1854 (1995); Shabaev V M *Phys. Rev. A* **57** 59 (1998); Adkins G S, Morrison S, Sapirstein J *Phys. Rev. A* **76** 042508 (2007)
25. Artemyev A N, Shabaev V M, Yerokhin V A *Phys. Rev. A* **52** 1884 (1995)
26. Plunien G, Soff G *Phys. Rev. A* **51** 1119 (1995); **53** 4614 (1996)
27. Nefiodov A V et al. *Phys. Lett. A* **222** 227 (1996)
28. Kozhedub Y S et al. *Phys. Rev. A* **77** 032501 (2008)
29. Klaft I et al. *Phys. Rev. Lett.* **73** 2425 (1994)
30. Crespo López-Urrutia J R et al. *Phys. Rev. Lett.* **77** 826 (1996); *Phys. Rev. A* **57** 879 (1998)
31. Seelig P et al. *Phys. Rev. Lett.* **81** 4824 (1998)
32. Beiersdorfer P et al. *Phys. Rev. A* **64** 032506 (2001)
33. Shabaev V M et al. *Phys. Rev. A* **56** 252 (1997)
34. Sen'kov R A, Dmitriev V F *Nucl. Phys. A* **706** 351 (2002)
35. Elizarov A A et al. *Nucl. Instrum. Meth. Phys. Res. B* **235** 65 (2005)
36. Shabaev V M et al. *Phys. Rev. Lett.* **86** 3959 (2001)
37. Häffner H et al. *Phys. Rev. Lett.* **85** 5308 (2000)
38. Shabaev V M *Phys. Rev. A* **64** 052104 (2001)
39. Shabaev V M, Yerokhin V A *Phys. Rev. Lett.* **88** 091801 (2002)
40. Yerokhin V A, Indelicato P, Shabaev V M *Phys. Rev. Lett.* **89** 143001 (2002)
41. Verdú J et al. *Phys. Rev. Lett.* **92** 093002 (2004)
42. Mohr P J, Taylor B N *Rev. Mod. Phys.* **77** 1 (2005)
43. Shabaev V M et al. *Phys. Rev. Lett.* **96** 253002 (2006)
44. Khriplovich I B *Phys. Scripta* **T112** 52 (2004)
45. Wood C S et al. *Science* **275** 1759 (1997); Bennett S C, Wieman C E *Phys. Rev. Lett.* **82** 2484; **83** 889 (1999)
46. Dzuba V A, Flambaum V V, Ginges J S M *Phys. Rev. D* **66** 076013 (2002)
47. Derevianko A *Phys. Rev. Lett.* **85** 1618 (2000)
48. Kozlov M G, Porsev S G, Tupitsyn I I *Phys. Rev. Lett.* **86** 3260 (2001)
49. Johnson W R, Bednyakov I, Soff G *Phys. Rev. Lett.* **87** 233001 (2001)
50. Kuchiev M Yu *J. Phys. B: At. Mol. Opt. Phys.* **35** L503 (2002); Kuchiev M Yu, Flambaum V V *Phys. Rev. Lett.* **89** 283002 (2002); *J. Phys. B: At. Mol. Opt. Phys.* **36** R191 (2003)
51. Milstein A I, Sushkov O P, Terekhov I S *Phys. Rev. Lett.* **89** 283003 (2002); *Phys. Rev. A* **67** 062103 (2003)
52. Shabaev V M et al. *Phys. Rev. Lett.* **94** 213002 (2005); *Phys. Rev. A* **72** 062105 (2005)
53. Flambaum V V, Ginges J S M *Phys. Rev. A* **72** 052115 (2005)
54. Rosner J L *Phys. Rev. D* **65** 073026 (2002)
55. Labzowsky L N et al. *Phys. Rev. A* **63** 054105 (2001)

PACS numbers: 06.20.Jr, 06.30.Ft, 12.20.Fv, 32.10.Fn, 32.30.Jc, 42.62.Fi
DOI: 10.1070/PU2008v051n11ABEH006644

High-precision laser spectroscopy of cold atoms and the search for the drift of the fine structure constant

N N Kolachevsky

1. Introduction

This review presents the main scientific results obtained over the last several years at the Laboratory of Active Media Optics of the Optical department of the Lebedev Physical Institute. The work was aimed at the search for and the investigation of high-finesse optical resonances in atomic ensembles. This allows carrying out sensitive tests of fundamental physical theories and opens the possibility of creating prospective frequency references in the optical range. A new laboratory method has been presented to search for the drift of the fine structure constant by using a frequency comb of a femtosecond laser, and sensitive experiments are being performed on testing the quantum electrodynamic theory. Work has started on laser cooling of the thulium atom, which experiences a narrow transition near 1.14 μm. The possibility of cooling was analyzed experimentally and theoretically, and the transitions most promising for the cooling were determined. A new generation of ultrastable optical cavities was developed for stabilizing the frequency of laser systems, which allows detecting optical resonances with a sub-Hertz resolution. A compact magneto-optical trap for rubidium atoms was created, and the interaction of femtosecond-laser radiation with a laser-cooled ensemble of atoms was investigated.

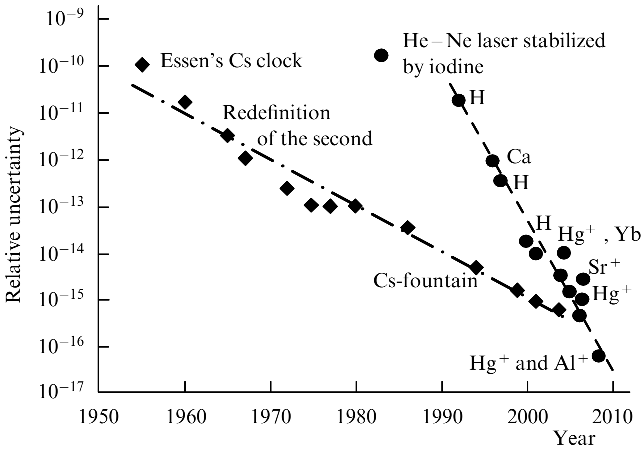

Figure 1. Uncertainty evolution for microwave (rhombs, dash-dotted line) and optical (circles, dashed line) frequency references. Noticeable progress in the development of optical standards is related to the evolution of new ultrastable laser systems, methods for measuring and comparing optical frequencies by means of an optical comb, and the development of new spectroscopic objects based on captured and cooled atoms and ions.

High-precision laser spectroscopy and laser cooling of atomic ensembles are rapidly developing fields of modern physics. In the last decade, the most impressive achievements have been awarded Nobel prizes for physics, specifically, the development of methods for cooling and trapping atoms by laser radiation (1997), the experimental discovery of Bose – Einstein condensation in dilute gases of alkali metals (2001), and the contribution to the development of methods for high-precision spectroscopy and the creation of a frequency comb on the basis of a femtosecond laser (2005) [1]. Intense investigations in the field of high-precision spectroscopy and metrology started about 30 years ago [2, 3]; however, it took a long time to approach the measurement uncertainty of $10^{-17} - 10^{-18}$, envisaged in pioneering works by A L Shavlov, V P Chebotaev, V S Letokhov, T W Hänsch, J L Hall, and other classics of nonlinear laser spectroscopy. As the result of long-term work, scientists from metrological and laser centers in the USA, Germany, Russia, France, England, and other countries succeeded in reducing the relative error of optical frequency references to 2×10^{-17} [4], which is by an order of magnitude better than the accuracy of the best primary standards, namely, cesium fountains [5]. In Fig. 1a, the relative errors of microwave and optical standards are compared.

Rapid progress in optical standards is mainly related to the development of simple-to-use laser systems with superior characteristics, which satisfy the most stringent requirements of experimenters. Laser systems are used for cooling and capturing atoms and ions in traps, for preparing their internal states, and in the spectroscopy of ultra-narrow 'clock'

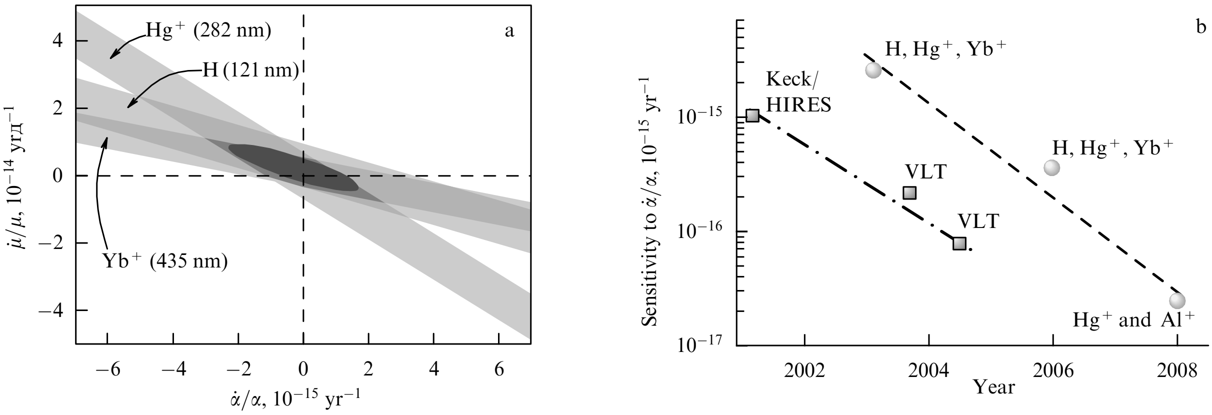

Figure 2. (a) Model-independent method for the search for a possible drift of fundamental constants based on a combined analysis of independent results on measuring the frequencies of absolute transitions in atoms and ions. The ellipse denotes the confidence interval (1σ) for the relative drifts of the fine structure constant $\dot{\alpha}/\alpha$ and the reduced magnetic moments $\dot{\mu}/\mu$ of the ^{133}Cs nucleus. (b) Comparison of the sensitivities of astrophysical (squares, dash-dotted line) and laboratory (circles, dashed line) methods to a possible linear drift of the fine structure constant.

transitions in single ions (see, e.g., [6, 7]), ensembles of laser-cooled neutral atoms [8, 9], and atomic beams [10, 11]. Principally new schemes are being developed for cooling, capturing, and spectroscopic measurements of atoms [4, 12, 13], which allow carrying out investigations at minimal influence of external perturbations on clock transitions. In turn, the use of a comb of optical frequencies based on the femtosecond laser with passive mode locking [14] opens the possibility of directly comparing reference frequencies in the RF and optical ranges, linking them by a simple and universal 'bridge.'

Such high-precision measurements and frequency comparison in the optical range not only are an important frontier in modern metrology but also open new possibilities for performing sensitive tests of fundamental theories. A relevant problem in modern physics is the question of the temporal stability of fundamental constants, in particular, the fine structure constant α. More than 70 years ago, Dirac [15] posed the question on the stability of α, which touches on the fundamentals of physical theories. The question has no answer yet, although the investigations in this field continue. A number of theories allow a possible drift of the coupling constant for electromagnetic interactions (see, e.g., reviews [16–18]), but the problem concerning the search for the drift resides in the experimental domain because no theory predicts the drift value.

In 2003, we measured the absolute frequency of the clock 1S$-$2S transition in the hydrogen atom (H) with the accuracy up to the 14th decimal place [19]. On this basis, a new laboratory model-independent method was developed for determining the possible drift of α, which is schematically shown in Fig. 2a [20]. The method suggests the experimental limitation on the drift of the frequencies of optical transitions measured relative to the frequency of a primary standard by means of a frequency comb. In addition, the different sensitivity of the transition frequencies to the parameter α due to relativistic effects [21] is taken into account. Data on the frequency of the 1S$-$2S transition in the hydrogen atom were used in a joint analysis with those from metrological centers in the USA (Hg^+ ion [22]) and Germany (Yb^+ ion [23]), which provided a bound on the drift of the fine structure constant at the level of $\dot{\alpha}/\alpha = (-0.9 \pm 2.9) \times 10^{-15}$ yr^{-1}. The sensitivity to the linear drift of α amounts to 3×10^{-15} yr^{-1} (the upper point in Fig. 2b), which is close to the accuracy of the analysis of quasar absorption spectra (under the assumption of a linear drift of α) performed by means of the complex Keck telescope/HIRES spectrometer (High Resolution Echelle Spectrometer) [24]. At the time, it was the strictest estimate obtained from the analysis of astrophysical data.

The results of the analysis in [24] indicated that about 10^{10} years ago, the parameter α differed from the modern value by $\Delta\alpha/\alpha = (-7.2 \pm 1.8) \times 10^{-6}$; this result stimulated further investigations in this area. In 2003–2004, the data obtained by the VLT (Very Large Telescope) were analyzed [25, 26], which, to the contrary, pointed to the invariability of α in the past relative to the present value, with the confidence level $|\Delta\alpha/\alpha| < 10^{-6}$. The collection of data detected from various astrophysical objects is inconsistent (for example, in Ref. [27], a nonzero drift is reported for the electron-to-proton mass ratio), which suggests that further investigations are necessary.

Nevertheless, the laboratory method developed in Ref. [20] based on the measurements of the absolute frequencies of clock transitions in various atomic systems by means of a femtosecond frequency comb allowed increasing the sensitivity to a linear drift by an order of magnitude already in 2005 (see Fig. 1b) [28, 29]. Presently, the drift of α is most strictly limited by a group from the National Institute of Standards and Technology (NIST) USA, who used a femtosecond comb to directly compare the frequencies of clock transitions in mercury and aluminum ions. It was found that the drift is bounded at the level $\dot{\alpha}/\alpha = (-1.6 \pm 2.3) \times 10^{-17}$ yr^{-1}, which is approximately an order of magnitude lower than the sensitivity of the best astrophysical tests [4]. A greater number of independent data, measurements of clock transitions in strongly relativistic systems, and an increased measuring duration have given the chance to enhance the sensitivity of laboratory methods to 10^{-18} yr^{-1} within the next few years and potentially to 10^{-20} yr^{-1}.

Some years ago, our group (Lebedev Physical Institute) suggested a new reference set of optical frequencies based on the dipole-forbidden transition at the wavelength 1.14 μm in the thulium atom. A potential finesse of this resonance reaches 2×10^{14}, and we therefore anticipate measuring the frequency in a cloud comprising $10^5 - 10^6$ atoms with an

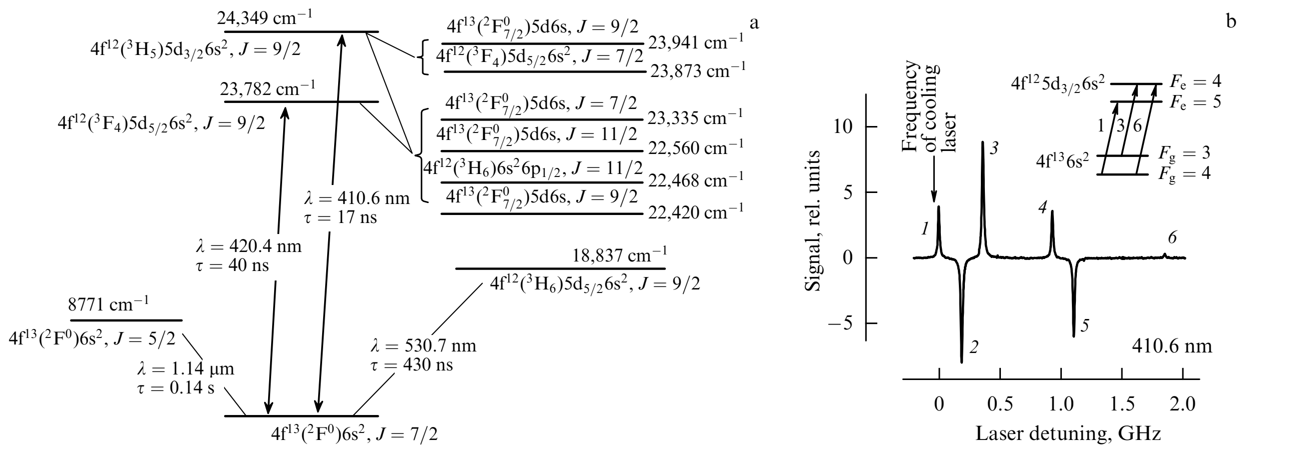

Figure 3. (a) Schematic diagram for thulium atom levels. (b) Experimentally recorded spectrum of saturated absorption at the wavelength $\lambda = 410.6$ nm. The required stabilized frequency for a cooling laser is shown.

accuracy comparable to that for standards on single ions and neutral atoms in optical lattices. Thus, we can obtain independent information on the bound on the drift of α by means of a high-relativistic thulium atom. Detection of resonances with a Hertz resolution requires a long-duration interaction of an atomic ensemble with laser radiation, which is only possible if atoms are cooled and localized. The spectroscopy of clock transition also requires the development of an ultrastable laser system. The thulium atom is widely used as a doping element in fiber and solid-state lasers, but the possibility of laser cooling and high-precision spectroscopy for this atom has not been considered so far.

In this review, we describe the strides towards solving the problem discussed. In Section 2, we investigate the possibility of laser cooling for the thulium atom using the results of sub-Doppler spectroscopy. In Section 3, the achievements of our group are presented on stabilizing laser systems by external reference cavities and some results are briefly described on using ultrastable laser systems in hydrogen atom spectroscopy. Section 4 is devoted to investigation results on the interaction of femtosecond radiation with an ensemble of laser-cooled rubidium-87 atoms in a magneto-optical trap.

2. Possibility of laser cooling for thulium

In the last decade, noticeable progress has been achieved in laser cooling of rare-earth elements. Compared to cooling by a buffer gas in a magneto-dipole trap demonstrated in Ref. [30], laser cooling exhibits lower temperatures, provides spectroscopy of narrow transitions almost free of external perturbations, and allows manipulation with separate atoms and groups of atoms. Despite the difficulty caused by the complicated structure of the spectra of lanthanides, scientific teams from the USA demonstrated laser cooling of ytterbium [31] and erbium [32] atoms in transitions residing in the blue spectral range (400 nm). The interest in rare-earth elements is explained by their prospective use in metrology and the study of ultra-narrow resonances [9], collision investigations at ultra-low temperatures and in Bose-condensates [33], and the possibility of implanting these atoms into solid substrates for solving problems in nanotechnology [34] and quantum informatics [35].

2.1 Study of cooling transitions

The thulium atom (Tm) has an electron vacancy in the 4f shell [the ground state configuration is $4f^{13}6s^2(^2F^0)$]. A natural isotopic mixture comprises only one isotope ^{169}Tm with the nuclear spin $I = 1/2$, which causes splitting of each electron level into two hyperfine-structure components. The ground state of the thulium atom comprises two fine-structure components (see Fig. 3a) with the quantum numbers $J_g = 7/2$ and $J'_g = 5/2$ of the total momentum of an electron shell with the splitting interval 2.6×10^{14} Hz ($\lambda = 1.14$ μm). Because the electron dipole transition between these sublevels is forbidden, it may be hoped that the $J'_g = 5/2$ state is long-lived (with the lifetime up to several tenths of a second). It is shown in [30, 36] that due to screening of the 4f shell by the external completed $6s^2$ shell, the influence of collisions on the frequency of the transition between the $J_g = 7/2$ and $J'_g = 5/2$ components of the ground state noticeably reduces.

The cooling of atoms is obligatory in creating a modern high-precision frequency reference because it eliminates the Doppler effect, provides a long period for their interaction with radiation, and allows the study of transitions virtually without external fields. For laser cooling of atoms, it is necessary to excite an intense cyclic transition that can be saturated by laser radiation. For the thulium atom, these may be dipole-allowed transitions from the sublevel ($J_g = 7/2$, $F = 4$) of the ground state $4f^{12}6s^2$ to the excited levels with ($J_e = 9/2, F = 5$), where F is the quantum number of the total momentum of the atom.

Among the excited levels of Tm, we can choose the following three candidates satisfying the criteria mentioned: $4f^{12}(^3H_6)5d_{5/2}6s^2$ (18,837 cm^{-1}), $4f^{12}(^3F_4)5d_{5/2}6s^2$ (23,782 cm^{-1}), and $4f^{12}(^3H_5)5d_{3/2}6s^2$ (24,349 cm^{-1}). The transition with the longest wavelength $\lambda = 530.7$ nm that can be excited by a second harmonic of the Nd:GSGG (Gadolinium Scandium Gallium Garnet) laser is totally cyclic; however, its relatively low probability $A = 2.3 \times 10^6$ s^{-1} prevents trap loading from atomic beams at room temperature. Nevertheless, this transition can be efficiently used with preliminarily cooled atoms. Two of the other transitions at the wavelengths 420.4 nm and 410.6 nm, which can be excited by a second harmonic of a Ti:sapphire laser, have noticeably greater probabilities (2.43×10^7 s^{-1} and 6.36×10^7 s^{-1} respectively [37]). This is sufficient for stopping atoms with velocities 200 m s^{-1} at a distance of

Table 1. Hyperfine splitting of the excited states in the thulium atom in our investigation [38]. Hyperfine splitting of the fundamental state is also presented.

Energy, cm^{-1}	Level	J	Splitting, MHz	References
0	$4f^{13}6s^2(^2F^0)$	7/2	−1496.550(1)	[39]
23,781.698	$4f^{12}(^3F_4)5d_{5/2}6s^2$	9/2	−1586.6(8)	[38]
23,873.207	$4f^{12}(^3F_4)5d_{5/2}6s^2$	7/2	+1411.0(7)	[38]
24,348.692	$4f^{12}(^3H_5)5d_{3/2}6s^2$	9/2	−1856.5(2,5)	[40]
			−1857.5(8)	[38]
24,418.018	$4f^{13}(^2F^0_{7/2})6s6p(^1P^0_1)$	5/2	−1969.4(1,3)	[38]

several tens of centimeters. The transitions are not fully cyclic, and there is a probability of the excited states decaying into the nearest levels of the opposite parity (see Fig. 3a).

We carried out a series of experiments and concluded that laser cooling of thulium atoms is possible.

The transitions with $\lambda = 420.4$ nm and $\lambda = 410.6$ nm were studied by means of saturation laser spectroscopy with counter-propagating beams of equal frequencies [38]. A sample spectrum is shown in Fig. 3b. The transitions were excited by the second harmonic of a Ti:sapphire laser. Thulium vapors were created by a vacuum oven heated to 700 °C.

The hyperfine splitting of excited states was determined for the transitions under study. For some transitions, this was made for the first time; for others, the error was reduced by several times (see Table 1). This investigation allows identifying the lines and adjusting the laser to the frequency necessary for laser cooling. The conclusion is made that in this scheme of levels, a swap laser is most likely unnecessary. In addition, the decay constants for the upper levels were specified, which determine the rate of atom cooling and the Doppler limit for a laser-cooled ensemble.

To determine the branching factor for the transitions under study (the ratio of the probability of unfavored decays for upper levels (see Fig. 3a) to the total decay probability), the individual probabilities were calculated for each pair of levels with opposite parities. The Cowan software package [41] was used for this purpose, which provides energy level calculations for multielectron neutral atoms and the corresponding transition probabilities. It was found that the branching factors for the transitions under study are

$$k_{410\ \mathrm{nm}} = 1^{+1}_{-0.5} \times 10^{-5}\,, \tag{1}$$

$$k_{420\ \mathrm{nm}} = 5^{+5}_{-2.5} \times 10^{-5}\,. \tag{2}$$

Because 35,000 photons should be scattered in order to cool a thulium atom with the initial velocity 200 m s^{-1}, the loss of atoms in the cooling cycle is about 97% (conservatively) for the $\lambda = 420.4$ nm transition and 50% for $\lambda = 410.6$ nm. Thus, the transition $\lambda = 410.6$ nm is preferable for laser cooling of thulium atoms and capturing them by a magneto-optical trap (MOT). The calculation for the Zeeman cooler was performed [42] and the results led us to the conclusion that about 5% of atoms in the atomic beam at the temperature 1100 K might be cooled by a laser to the temperature corresponding to the velocity 20 m s^{-1} and then captured by the MOT.

The probability of the magneto-dipole transition between fine sublevels of the ground state was calculated. This probability is $A = 7(2)$ s^{-1}, which corresponds to the natural linewidth 1.3 Hz and the transition Q-factor 2×10^{14}.

2.2 Conclusions

Laser-cooled thulium atoms are promising for solving problems in high-precision spectroscopy. The substantial screening of the 4f shell allows detecting narrow lines in dense atomic ensembles with discrete atomic-like spectra even if they are implanted into solid substrates. For example, the clock transition with $\lambda = 1.14$ μm, having the finesse 2×10^{14}, is strongly screened against collisions [36], which opens the possibility of detecting narrow unperturbed resonances in a dense cloud of atoms captured by a magneto-optical trap.

We have shown that efficient laser cooling of thulium can be realized by using the radiation tuned with the transition

$$4f^{13}6s^2(F=4) \rightarrow 4f^{12}(^3H_5)5d_{3/2}6s^2(F=5)$$

at the wavelength 410.6 nm. It is likely that a repumper laser would not be needed in this case. The calculation shows that at the temperature 1100 K, about 5% of atoms in the thermal beam can be decelerated to velocities 20 m s^{-1} and then captured by a magneto-optical trap. In this case, about 10^6 atoms can be captured in the trap at the temperature $T_D = 230$ μK (the Doppler limit). Further cooling of atoms is possible either by means of sub-Doppler cooling or by switching to the transition with the wavelength 530.7 nm, which corresponds to $T_D = 9$ μK.

Presently, we are working on creating a magneto-optical trap for thulium atoms.

3. Stabilizing lasers at a sub-Hertz level

For studying narrow optical transitions in atomic systems, laser sources are needed with characteristics not limiting the resolution of the system. To detect Hertz-width resonances (see, e.g., Refs [4, 9]), the laser frequency fluctuations must be within several tenths of a Hertz. This places exacting constraints on the design of reference cavities whose frequency is a reference for stabilizing the laser radiation frequency. Indeed, using the relation $\delta l/l = \delta\nu/\nu$ (where l is the cavity length and ν is the frequency of the laser field) for the cavity length $l = 0.1$ m, we obtain that the frequency changes by 1 Hz under the displacement of one of the cavity mirrors by less than 10^{-15} m, which equals the proton radius! Mirror vibrations, temperature variation, and fluctuations in the radiation power inside the cavity result in an instability of the cavity length and, hence, of the frequency of the laser stabilized. The creation of a compact and simple-to-use design of the reference cavity is a relevant problem, which determines the stabilization of the laser frequency at the sub-Hertz level.

3.1 Vertical cavities with temperature compensation

External active and passive systems designed for damping vibrations and temperature fluctuations in an ambient medium can only partially limit the influence of these factors, which is usually insufficient for satisfying the requirements considered above. Additional damping of fluctuations can be provided by a special construction of the cavity itself, which should be least sensitive to vibrations and temperature fluctuations. Several groups at the leading scientific centers are developing such systems (see, e.g., Refs [43, 49]). Noticeable progress in cavity stability was obtained through a special suspension whose plane passes through the center of mass of the system [43, 46].

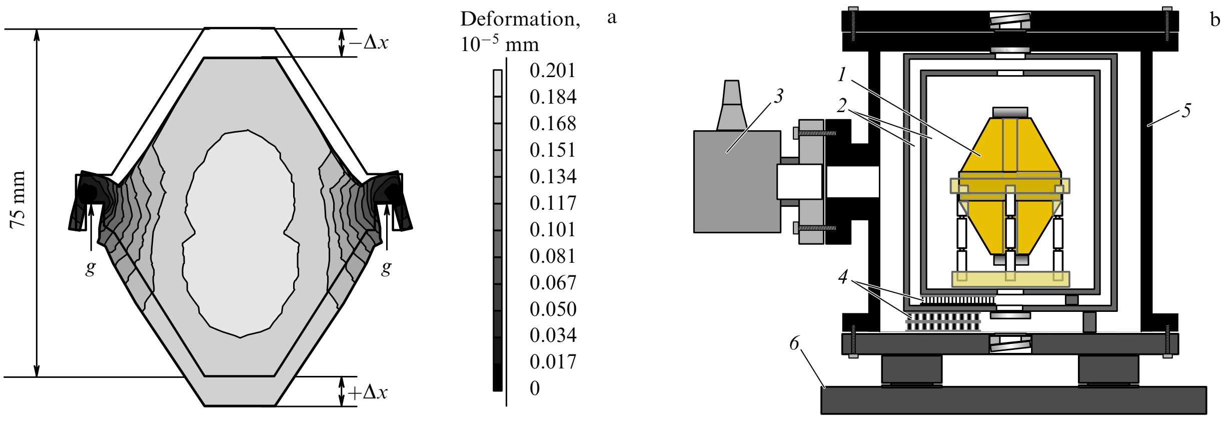

Figure 4. (a) Symmetric cavity with a vertical axis under the action of vertical acceleration. (b) Vertical cavity with the cooling and vacuum systems assembled: *1*, the cavity; *2*, the cooled duralumin screens; *3*, the getter-ion pump; *4*, Peltier elements; *5*, the vacuum chamber; *6*, the optical mount with an active system for suppressing vibrations.

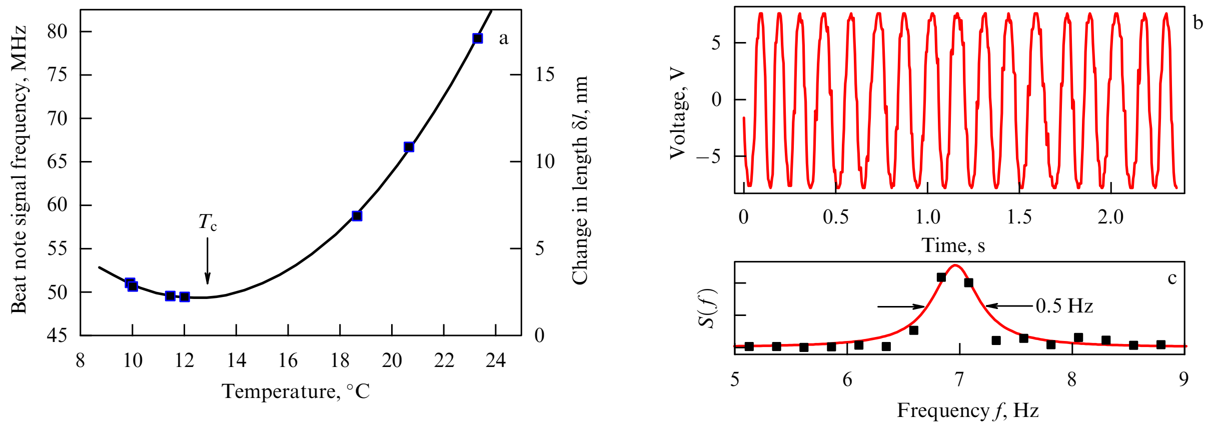

Figure 5. (a) Determination of the critical temperature T_c for a cavity made from ULE glass. (b) Oscillogram of the beat note signal for two lasers stabilized with respect to two independent cavities. (c) Spectral power density for the beat note signal presented in Fig. b.

Our group has combined the construction of a vertical cavity with the symmetric suspension shown in Fig. 4a. It can be seen that vertical acceleration reduces to a symmetric compression and tension of the top and bottom parts, respectively. The distance between cavity ends remains unchanged in the process. Such a construction of the cavity and suspension results in a weaker effect of vertical vibrations. Two mirrors with multilayer coatings, which provide the cavity finesse 4×10^5 at the wavelength 972 nm, are attached by an optical contact to the ends of the cavity made from special ULE glass (ultra low expansion glass [50]). This wavelength was chosen because it coincides with the fourth subharmonic of the radiation needed for a two-photon excitation of the 1S – 2S transition in the hydrogen atom (243 nm). The cavity is placed in a vacuum chamber, which is continuously evacuated by a getter-ion pump (see Fig. 4b). The residual vacuum in the chamber is 10^{-8} mbar. For reducing horizontal vibrations, the cavity was placed on an optical table supplied with an active system for damping vibrations.

An important factor affecting the cavity stability is fluctuations in the temperature of the ambient medium. Usually, cavities are supplied with complicated multistage systems for temperature compensation and are made from a special material having a minimal thermal expansion coefficient. For example, ULE glass exhibits the specific dependence of length on temperature expressed as

$$\frac{\delta l}{l} \sim 10^{-9}(T - T_c)^2 \,, \tag{3}$$

where T_c is the so-called critical temperature at which the length is minimal and the linear coefficient of thermal expansion vanishes. Usually, T_c is below room temperature and the system of external temperature stabilization cannot be used because of the moisture condensation. In fact, cooled cavities capable of providing laser stabilization for many days have not been used in practice yet.

We realized a method for cooling the cavity to T_c [49] by using Peltier elements placed in a vacuum chamber and multistage thermal screens (see Fig. 4b). The system for temperature stabilization is substantially simplified in this case and no condensation problem arises. A semiconductor laser in the Littrow configuration was stabilized with respect to the cavity transmission peak by means of an electronic feedback [51]. Two independent systems were made, which allowed carrying out experiments on determining T_c and studying the frequency stability of each of the systems.

In Fig. 5a, the frequency of the beat note signal is shown for two stabilized semiconductor lasers versus the tempera-

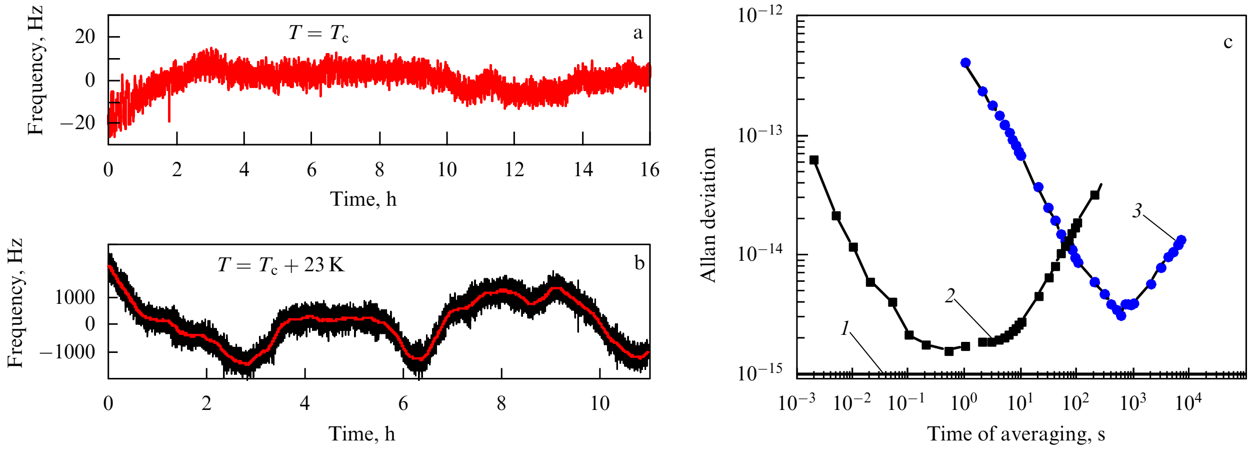

Figure 6. (a) The frequency of a cavity stabilized at the temperature T_c. The linear drift 63 mHz s^{-1} is subtracted. (b) Stability of the cavity frequency at the temperature $T_c + 23$ K. (c) Allan deviation graphs for the thermal noise of the cavity (curve *1*); for the beat note signal for two cavities, one of them stabilized at T_c and the other at $T_c + 23$ K (curve *2*); for the beat note signal for a cavity at T_c and the frequency comb stabilized by an active hydrogen maser (curve *3*).

ture of one of the cavities (see Fig. 4b). It can be seen that the cavity length is minimal at $T_c = 12.5\,°C$; hence, the cavity exhibits the least sensitivity to variations of the external temperature in this case. The stabilizing system maintains the temperature near T_c with an accuracy about 1 mK, which corresponds to the sensitivity of the cavity frequency to temperature variations at the level of 50 Hz mK^{-1}.

For studying the short-time frequency characteristics of a stabilized laser, we recorded the oscillogram of frequency beatings with heterodyne conversion to low frequencies (see Fig. 5b). Fourier analysis of the signal shows that the radiation spectral width of each of the lasers is below 0.5 Hz at the averaging time 2 s (see Fig. 5c).

To characterize the long-time stability and determine the drift characteristics of the cavity, we measured the laser frequency by means of a frequency comb stabilized by the signal from an active hydrogen maser. A laser stabilized with respect to the cavity at the temperature T_c exhibits an almost linear drift of the frequency, of the order of 50 mHz s^{-1}, which arises due to material aging (recrystallization). As can be seen from Fig. 6a, deviations from the linear drift do not exceed 20 Hz for a time lapse of approximately 10 hours. For comparison, we measured the drift characteristics for a cavity stabilized at a temperature much higher than the critical, at $T_c + 23$ K. The sensitivity to temperature fluctuations increases to ~ 10 kHz mK^{-1}. This fact is confirmed by experimental observations (see Fig. 6b).

The results of the full analysis of characteristics of the laser system created are presented in Fig. 6c in the form of the Allan deviation [52]. Two independent laser systems were used, one of them stabilized with respect to the frequency of the cavity at the temperature T_c and the other with respect to the frequency of the other cavity at $T_c + 23$ K (curve *2*). The relative instability of the total system reaches 2×10^{-15} in the time interval 0.1 – 10 s, approaching the fundamental limit for cavity thermal noise (curve *1*) [53]. The cavity stability at T_c is also characterized by using a frequency comb (curve *3*). The measurements show that the instability of the laser system remains at the level of several units in the fifteenth digit for the time lapse of several hundred seconds.

3.2 Measurement of hyperfine splitting for the 2S level in a hydrogen atom

The laser system created was used for measuring the frequency of the hyperfine interval for the 2S level in the hydrogen atom. High-precision measurement of the frequency $f_{HFS}(2S)$ of this interval allows carrying out a sensitive test for small quantum mechanical contributions [54, 55] based on the analysis of the specific difference $D_{21} = 8 f_{HFS}(2S) - f_{HFS}(1S)$ [56].

Earlier, we suggested a new method for measuring $f_{HFS}(2S)$ by two-photon spectroscopy on the 1S–2S transition in the hydrogen atom [54]. As can be seen from Fig. 7a, the relation

$$f_{HFS}(2S) = f_{HFS}(1S) + f_{triplet} - f_{singlet} \quad (4)$$

holds in vanishing magnetic fields, where $f_{triplet}$ and $f_{singlet}$ are the frequencies of triplet and singlet two-photon transitions. Hence, the problem of measuring the hyperfine splitting of the 2S level reduces to finding the difference between two optical frequencies because the value of $f_{HFS}(1S)$ is known to the 13th decimal place [57].

The method of measurements of $f_{HFS}(2S)$ used in 2008 is similar to that in [54], with the difference being that for a nonabsolute stable optical-frequency reference, we used the radiation of a diode laser with $\lambda = 972$ nm stabilized with respect to the cavity described in Section 3.1. The measurement results are presented as a histogram in Fig. 7b. The histogram is described by a Gaussian distribution with the width 85 Hz. We note that so small a statistical deviation is obtained in subtracting two optical frequencies of 2.26×10^{15} Hz each. The result of preliminary data processing gives $f_{HFS}(2S) = (177{,}556{,}840 \pm 5)$ Hz [58], which considerably refines the result $(177{,}556{,}860 \pm 16)$ Hz of the previous optical measurement carried out in 2003 [54]. We note that the new result, which is five times more accurate than that obtained by the direct radiofrequency method $(177{,}556{,}785 \pm 29)$ Hz [59] allows analyzing small (at the level of $< 10^{-7}$) corrections to the quantum electrodynamics of bound states in light atoms, and thus naturally complements tests based on an analysis of the Lamb shift.

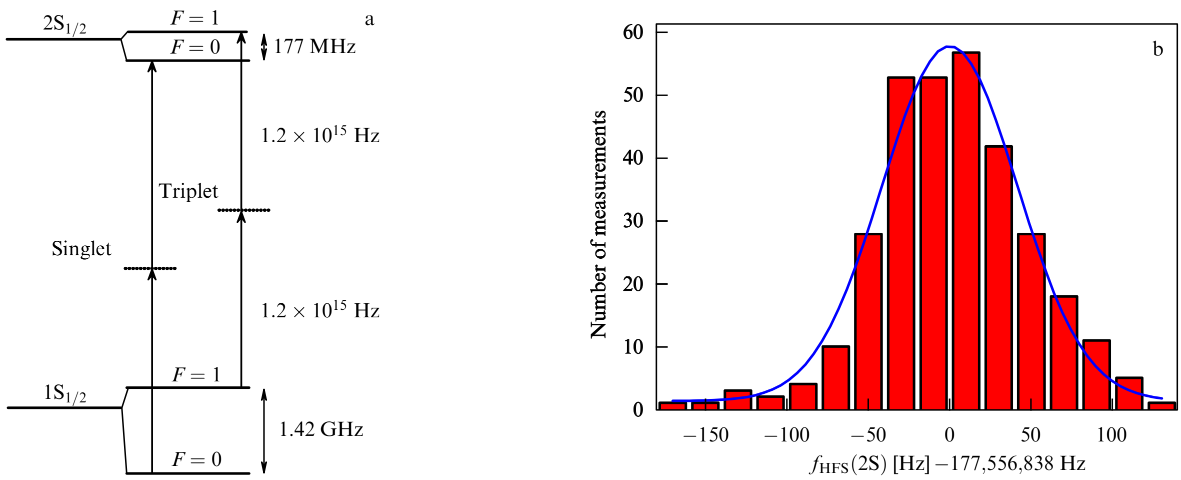

Figure 7. (a) Schematic diagram of measuring the hyperfine splitting for the 2S level by two-photon spectroscopy of the 1S – 2S transition. (b) Hystogram of the measuring results for $f_{HFS}(2S)$ in the hydrogen atom and its approximation by a Gaussian profile.

3.3 Conclusions

New kinds of vibration- and temperature-compensated reference cavities capable of stabilizing laser systems with a sub-Hertz accuracy have been developed and realized. Such compact systems with typical dimensions $50 \times 50 \times 50$ cm^3 allow studying clock transitions in various atomic systems. We plan to use reference cavities of such a construction in the spectroscopy of clock transitions in thulium ($\lambda = 1.14$ μm) and hydrogen ($\lambda = 0.92$ μm) atoms. A laser system has been created with the wavelength $\lambda = 972$ nm, the spectral line width less than 0.5 Hz, the monotonic drift about 50 mHz s^{-1}, and the frequency instability below 5×10^{-15} over a time lapse in the range 0.1 – 100 s. At such durations, the frequency instability of the laser system is actually completely determined by the fundamental limit of the thermal noise of the reference cavity kept at a temperature about 300 K.

Using this laser system at the wavelength $\lambda = 972$ nm, we measured the hyperfine splitting of the 2S level in the hydrogen atom, which allows testing small corrections to the quantum electrodynamics of bound states. The result of preliminary processing of data measured in 2008 is $f_{HFS}(2S) = (177{,}556{,}840 \pm 5)$ Hz, which is five times better than the result obtained earlier by a direct radiofrequency measurement [59].

4. Interaction of laser-cooled ^{87}Rb with femtosecond radiation

Laser cooling of atoms opens unique possibilities for studying their intrinsic states. Most high-precision spectroscopic investigations are presently carried out with the help of laser cooling methods. For example, the use of such methods in cesium fountains has increased the accuracy of cesium standards reproducing the time unit in the SI system of units by more than an order [5]. Atom cooling in optical frequency references down to temperatures about 10 μK almost completely eliminates the influence of the Doppler effect and the limitation related to the finite time of the interaction with radiation. The development of special methods capable of scanning for atoms either in the free-falling mode [8] or in optical gratings at a 'magical' wavelength [12] ensures a minimal influence of external fields on the clock transition frequency.

The long lifetime of laser-cooled atoms in the trap domain allows reliably detecting processes occurring in a characteristic time about 1 s, which cannot be done, for example, with atomic beams. One such process is, in fact, the excitation of a clock transition. In the thulium atom, for example, the expected excitation rate for the $\lambda = 1.14$ μm transition is 0.1 – 1 s^{-1}. Detection of such processes is possible either by using the method of quantum hops for a small number of trapped atoms [60] or by measuring the population of the ground state in a large ensemble. In both cases, the act of excitation is detected via the two-photon process, namely, absorption at the clock transition wavelength and luminescence in another transition, which is usually the cooling transition.

For studying multi-photon processes in a cloud of laser-cooled atoms, we created a MOT for ^{87}Rb atoms and analyzed the interaction of the cloud with radiation from a femtosecond laser.

4.1 Magneto-optical trap for ^{87}Rb

We have created a MOT for ^{87}Rb atoms (see, e.g., Ref. [61]). A distinguishing feature of the configuration of this MOT is the compactness and reliability of the system. Atoms are trapped in a rectangular glass cell evacuated to a pressure below 10^{-9} mbar. As the source of atoms, we used the special dispensers produced by SAES Getters capable of precisely controlling the flux of rubidium atoms by varying the dispenser current. The cooling laser radiation at the wavelength 780 nm [the $5S_{1/2}(F = 2) \rightarrow 5P_{3/2}(F = 3)$ transition in Fig. 8a] is generated by a semiconductor laser stabilized by a resonance transition in rubidium with the laser frequency differing from the atomic resonance frequency by -12 MHz. To avoid populating the 'dark' sublevel $F = 1$ of the ground state, we used an additional repumping laser. After thorough intensity balancing, beams of the laser pass from six directions onto a glass cell. The crossing center of the six beams matches the three-dimensional minimum of the magnetic field produced by two coils in an anti-Helmholtz configuration with the field gradient about 10 G cm^{-1}. MOT luminescence at the wavelength 780 nm is detected by a CCD camera and a calibrated photodiode.

The cloud of cold atoms has the diameter 200 μm (at the level $1/e^2$) as shown in Fig. 8b. At the maximal current

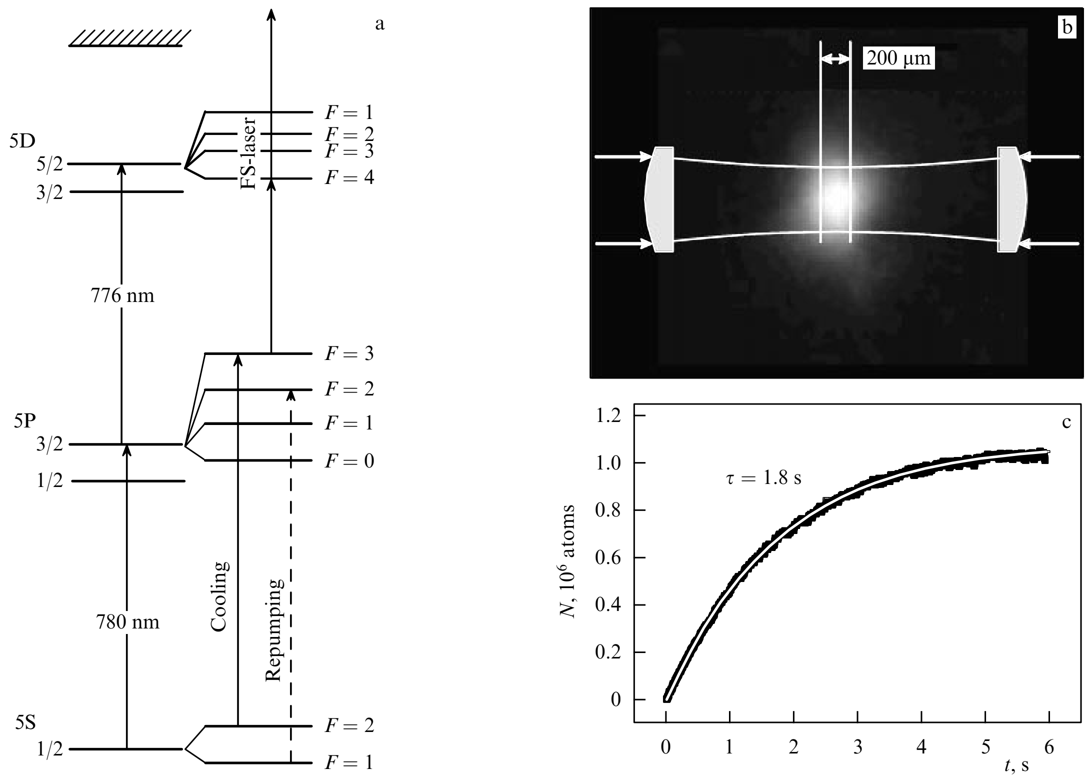

Figure 8. (a) Level structure of the ^{87}Rb atom used in the experiment. (b) MOT image at the wavelength of luminescence 780 nm. Focusing of femtosecond laser radiation is shown schematically. (c) Curve of trap loading. The approximation of experimental data by the exponential function of type (5) with the time constant $\tau = 1.8$ s is shown.

through the dispensers, the number of trapped atoms reaches 10^7, which corresponds to the cloud density 10^{12} cm^{-3}. The temperature of atoms measured by the method of recapture was 250 μK, which is close to the Doppler limit $h\gamma/2k_B = 140$ μK, where $\gamma = 6$ MHz is the cooling transition width.

An important MOT parameter is the atom lifetime in the trap domain. It can be determined from the characteristic time for trap load

$$N(t) = R\tau\left[1 - \exp\left(-\frac{t}{\tau}\right)\right], \qquad (5)$$

where N is the number of atoms in the MOT and R and τ are the capture rate and lifetime. At a low atom concentration, we can neglect the losses caused by atom collisions inside the MOT. As can be seen from Fig. 8c, the characteristic trap load time is $\tau = 1.8$ s at the dispenser current 4.5 A. The lifetime of atoms in the MOT is mainly affected by collisions with rubidium atoms emitted from the dispensers. A reduction in the current results in longer τ; however, the capture rate and the total number of atoms $N(t \to \infty)$ simultaneously decrease. The regime in which τ is about 2 s is optimal for reaching both the maximal number of atoms in the trap (about several million) and their longest lifetime. It follows from Eqn (5) and Fig. 8c that every process with the frequency exceeding 0.5 s^{-1} that expels atoms from the cooling cycle (collisions, pumping into 'dark states', ionization) would substantially influence the shape of the load curve similar to the curve presented in Fig. 8c. This opens the possibility for a detailed analysis of such processes.

4.2 Interaction with a field from a femtosecond laser

The present section is devoted to studying the interaction of atoms captured by a MOT with radiation from a femtosecond (fs) laser operating in a cw mode. The specific features of this interaction were theoretically considered more than 30 years ago; however, intensive experimental investigation in this field started not long ago. In 1977, Baklanov and Chebotaev [62] predicted the possibility of detecting narrow two-photon resonances with the spectral width corresponding to the natural width despite a considerable spectral width of the laser source (up to several tens of nm for fs lasers).

This fact is explained by the specific spectrum of such lasers, which is given by a comb of optical modes whose frequencies are

$$f_n = f_0 + n f_{\text{rep}}, \qquad (6)$$

where f_0 is the offset frequency caused by a difference in the group and phase velocities inside the laser cavity, f_{rep} is the laser pulse repetition frequency, and n is the mode number [14]. Successful use of fs lasers in spectroscopic studies of levels with the spectral width close to the natural width is demonstrated by the spectroscopy of anti-Stokes scattering [63], two-photon spectroscopy [64], and single-photon spectroscopy of atomic beams [65].

In our experiment, radiation from an fs laser ($f_{\text{rep}} = 76$ MHz, the pulse duration was 200 fs) was focused from opposite sides onto a cloud of atoms residing in a MOT (see Fig. 8b) with the beam waist $w_0 = 210$ μm overlapping the entire cloud. The central wavelength of the laser was 776 nm, which corresponds to the $5P_{3/2} \to 5D_{5/2}$ transition wavelength in ^{87}Rb (see Fig. 8a). Under variations in the

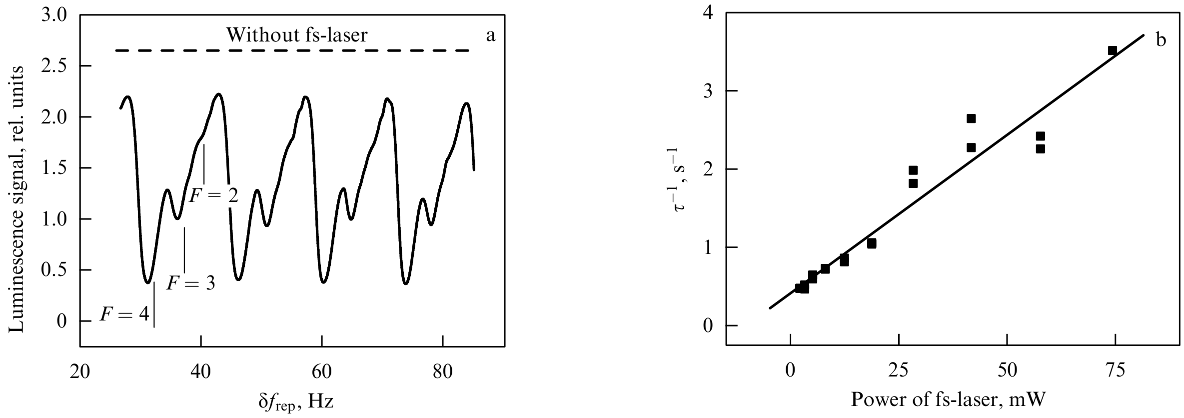

Figure 9. (a) Periodical dependence of MOT luminescence signal versus the detuning δf_{rep} of the repetition frequency of an fs laser. (b) Dependence of the atom inverse lifetime τ^{-1} on the power of fs laser radiation.

repetition frequency of the fs laser, periodic resonance variations of the luminescence signal for the $5P_{3/2}(F=3)$ level at the wavelength $\lambda = 780$ nm were detected as shown in Fig. 9a. The spectrum periodicity is explained by the periodicity of the fs-laser spectrum (6). Spectrum identification shows that the lines correspond to the $5P_{3/2}(F=3) \to 5D_{5/2}(F=2,3,4)$ transitions excited by separate modes of the fs laser from the upper populated level of the trap (see Fig. 8a). But so strong an effect resulting in the resonance depletion of the $5P_{3/2}(F=3)$ level and, correspondingly, in a tenfold suppression of luminescence cannot be explained in the framework of single-photon excitation because the light intensity power produced by the single mode of an fs-laser (6) is small in a cloud.

We analyzed this effect in a series of studies, where we separately investigated the effect of monochromatic radiation, mechanical action at the resonance transition, optical pumping, and ionization on the MOT excitation luminescence [66]. The conclusion was that a decrease in the number of atoms in a MOT is related to the two-photon process under which the atoms excited by a single mode of an fs laser and transiting to the $5D_{5/2}$ level are then ionized by the full power of the fs laser. The probability of this process is of the order of 1 to 10 s^{-1}, depending on the Fs laser power, and therefore the effect can be investigated based on the lifetime of atoms in the trap, Eqn (5).

To simplify interpretation of the phenomenon observed, the scheme of the experiment was modified. The $5P_{3/2}(F=3) \to 5D_{5/2}(F=4)$ transition was excited by a CW frequency-stabilized diode laser tuned to the transition ($\lambda = 776$ nm). The $5D_{5/2}$ level was ionized by the radiation from an fs laser whose central wavelength was tuned to 820 nm, free of Rb-atom resonances. Laser beams overlapped such that the spatial modes of the lasers coincided. In this case, the field of the fs laser, which does not itself affect the MOT, plays the role of a 'catalyst,' noticeably increasing the influence of the resonance field of the CW laser. In Fig. 9b, the inverse lifetime for an atom in the MOT is shown versus the radiation power of the fs laser. The power of the CW laser remained constant.

From experimental data on the known effective ionization cross section $\sigma_{\text{eff}} = (1.2 \pm 0.2) \times 10^{-17}$ cm^2 for the $5D_{5/2}$-level [67], we succeeded in determining the efficiency of exciting the $5P_{3/2}(F=3) \to 5D_{5/2}(F=4)$ transition with the field of the CW laser with a power P_{776} in our experimental configuration. It was found that the efficiency is $\vartheta = (1.9 \pm 0.5) \times 10^{-4} P_{776}$ [μW^{-1}]. Despite the relatively high uncertainty, this method proves to be substantially more precise than direct determination of the level population by luminescence, which is especially difficult in the case of weak signals. The fraction of atoms passing to the $5D_{5/2}$ level as the result of excitation by a single mode of the fs laser with the average power 100 mW and the central wavelength 776 nm is 3×10^{-4}. This corresponds to the total number of excited atoms about 300.

4.3 Summary

The compact magneto-optical trap is created for rubidium-87 atoms, capable of capturing about $10^6 - 10^7$ atoms with the density $10^{11} - 10^{12}$ cm^{-3} at the temperature 250 μK. The lifetime of an atom in the trap is about 2 s, which gives the possibility to quantitatively study weak processes with the characteristic frequency above 0.5 s^{-1}.

It is shown that the interaction of atoms with the field of a passive mode-locked femtosecond laser at the central wavelength 776 nm is of a resonance character. The strong resonances observed in the experiments are explained by the excitation of the $5P_{3/2} \to 5D_{5/2}$ transition by a single mode of the fs laser and then by the ionization of the $5D_{5/2}$ level, which results in atoms being expelled from the cooling cycle. The width of resonances observed is close to the natural transition widths. By measuring the time constant for the trap load curve, we quantitatively interpreted this two-photon process and developed a sensitive method for determining the population of the $5D_{5/2}$ level in ^{87}Rb. The method allows a confident detection of the transition of several hundred excited atoms in a cloud to an upper electron level without collecting luminescence photons from this level, which is important in studying strongly forbidden clock transitions.

The methods developed are needed for solving problems at the next stage, such as studying the excitation of the two-photon metrological $5S_{1/2} \to 5D_{5/2}$ transition (778 nm) in ^{87}Rb with the field of a femtosecond laser and spectroscopy of laser-cooled thulium atoms (see Section 2). Substantial experience was acquired in working with laser-cooled atoms and the possibility was experimentally demonstrated to quantitatively analyze weak processes of interaction with radiation, which include the excitation of the clock transition.

5. Conclusion

A series of works is being performed with the aim of developing a new optical frequency reference for studying the time variation of the fine structure constant α. As a possible object for investigations, we suggested the metrological transition at the wavelength 1.14 μm in the strongly relativistic ^{169}Tm atom, whose frequency is weakly affected by a collisional shift. The possibility of laser cooling of a thulium atom was studied and was shown to be feasible for the transition at the wavelength 410 nm. A laser system was created whose frequency matches that of the cooling transition. Under construction are a magnetic system of a Zeeman cooler, a vacuum chamber, and an optical system for cooling and capturing atoms with a magneto-optical trap.

A new generation of optical cavities has been developed and created with low sensitivity to temperature fluctuations and vibrations. The spectral width of a semiconductor laser ($\lambda = 972$ nm) stabilized relative to such a cavity is below 0.5 Hz at the frequency drift about 50 mHz s^{-1}. The hyperfine splitting frequency $f_{\mathrm{HFS}}(2\mathrm{S}) = (177{,}556{,}840 \pm 5)$ Hz for the 2S-level in the hydrogen atom (a preliminary result) was measured by using such a laser system, which opens the possibility of performing sensitive tests in quantum electrodynamics. A similar laser system was developed for the spectroscopy of the clock transition in the ^{169}Tm atom.

A compact magneto-optical trap was created for ^{87}Rb atoms and the interaction of laser-cooled atoms with a femtosecond radiation was studied. It has been experimentally shown that weak processes with the characteristic rates down to 0.5 s^{-1} can be studied quantitatively by measuring the characteristic load time for the trap. The methods developed open the possibility of detecting the weak clock transition in thulium atoms.

The use of new objects in spectroscopic investigations, laser systems, and methods for measuring clock transitions is likely to favor achieving, within the next few years, sensitivity to the drift of the fine structure constant at the level of $\dot{\alpha}/\alpha \sim 10^{-18}$ yr^{-1}. This brings laboratory methods to a leading position in studying the drift of α in the modern age of the evolution of the Universe.

Acknowledgements

The author expresses his deep appreciation to young collaborators from Laboratory of Active Media Optics A V Akimov and A V Sokolov, students and graduate students of MIPT A N Matveev, E O Tereshchenko, A Yu Samokotin, K A Chebakov, P B Rodionov, and M V Egorov involved in the projects presented in this review. The author is especially grateful to the head of the laboratory V N Sorokin for his constant help, and to his LPI collaborators S I Kanorskii and I Yu Tolstikhina. The author is grateful to T W Hänsch for the hospitality and the opportunity to solve scientific problems in quantum optics at the laboratory of the Max-Planck Institute. This work was supported by the RFBR (08-07-00127), the grant of the President of Russian Federation MD-887.2008.2, the Russian Science Support Foundation, DFG, and the Alexander von Humboldt Foundation.

References

1. The Nobel Prize in Physics, http://nobelprize.org/nobel_prizes/physics/
2. Letokhov V S, Chebotaev V P *Printsipy Nelineinoi Lazernoi Spektroskopii* (Principles of Nonlinear Laser Spectroscopy) (Moscow: Nauka, 1975)
3. Bagaev S N, Chebotaev V P *Usp. Fiz. Nauk* **148** 143 (1986) [*Sov. Phys. Usp.* **29** 82 (1986)]
4. Rosenband T et al. *Science* **319** 1808 (2008)
5. Bize S et al. *J. Phys. B: At. Mol. Opt. Phys.* **38** S449 (2005)
6. Tamm Chr, Engelke D, Bühner V *Phys. Rev. A* **61** 053405 (2000)
7. Diddams S A et al. *Science* **293** 825 (2001)
8. Oates C W et al. *Eur. Phys. J. D* **7** 449 (1999)
9. Barber Z W et al. *Phys. Rev. Lett.* **96** 083002 (2006)
10. Barger R L *Opt. Lett.* **6** 145 (1981)
11. Kolachevsky N et al. *Phys. Rev. A* **73** 021801(R) (2006)
12. Katori H et al. *Phys. Rev. Lett.* **91** 173005 (2003)
13. Wineland D J et al. "Quantum computers and atomic clocks", in *Proc. of the 6th Symp. on Frequency Standards and Metrology* (Ed. P Gill) (Singapore: World Scientific, 2002) p. 361
14. Udem Th, Holzwarth R, Hänsch T W *Nature* **416** 233 (2002)
15. Dirac P A M *Nature* **139** 323 (1937)
16. Karshenboim S G *Can. J. Phys.* **78** 639 (2000)
17. Varshalovich D A et al. "Current status of the problem of cosmological variability of fundamental physical constants", in *Precision Physics of Simple Atomic Systems* (Lecture Notes in Physics, Vol. 627, Eds S G Karshenboim, V B Smirnov) (Berlin: Springer-Verlag, 2003) p. 199
18. Uzan J-P *Rev. Mod. Phys.* **75** 403 (2003)
19. Fischer M et al. *Phys. Rev. Lett.* **92** 230802 (2004)
20. Kolachevsky N N *Usp. Fiz. Nauk* **174** 1171 (2004) [*Phys. Usp.* **47** 1101 (2004)]
21. Dzuba V A, Flambaum V V, Webb J K *Phys. Rev. A* **59** 230 (1999)
22. Marion H et al. *Phys. Rev. Lett.* **90** 150801 (2003)
23. Peik E et al. *Phys. Rev. Lett.* **93** 170801 (2004)
24. Webb J K et al. *Phys. Rev. Lett.* **87** 091301 (2001)
25. Srianand R et al. *Phys. Rev. Lett.* **92** 121302 (2004)
26. Quast R, Reimers D, Levshakov S A *Astron. Astrophys.* **415** L7 (2004)
27. Reinhold E et al. *Phys. Rev. Lett.* **96** 151101 (2006)
28. Kolachevsky N et al. "Precision measurements in atomic hydrogen", in *Optical Standards on Neutral Atoms* (Ed. Yu Ovchinnikov) (in press)
29. Lea S N *Rep. Prog. Phys.* **70** 1473 (2007)
30. Hancox C I et al. *Nature* **431** 281 (2004)
31. Maruyama R et al. *Phys. Rev. A* **68** 011403 (2003)
32. McClelland J J, Hanssen J L *Phys. Rev. Lett.* **96** 143005 (2006)
33. Takasu Y et al. *Phys. Rev. Lett.* **91** 040404 (2003)
34. Hill S B, McClelland J J *Appl. Phys. Lett.* **82** 3128 (2003)
35. Monroe C *Nature* **416** 238 (2002)
36. Aleksandrov E B et al. *Opt. Spektrosk.* **54** 3 (1983) [*Opt. Spectrosc.* **54** 1 (1983)]
37. Wickliffe M E, Lawler J E *J. Opt. Soc. Am. B* **14** 737 (1997)
38. Kolachevsky N et al. *Appl. Phys. B* **89** 589 (2007)
39. Childs W J et al. *J. Opt. Soc. Am. B* **1** 22 (1984)
40. Kröger S et al. *Z. Phys. D* **41** 181 (1997)
41. Cowan R D *The Theory of Atomic Structure and Spectra* (Berkeley, CA: Univ. of California Press, 1981), and Cowan programs RCN, RCN2, and RCG
42. Barrett T E et al. *Phys. Rev. Lett.* **67** 3483 (1991)
43. Notcutt M et al. *Opt. Lett.* **30** 1815 (2005)
44. Ludlow A D et al. *Opt. Lett.* **32** 641 (2007)
45. Chen L et al. *Phys. Rev. A* **74** 053801 (2006)
46. Nazarova T, Riehle F, Sterr U *Appl. Phys. B* **83** 531 (2006)
47. Webster S A, Oxborrow M, Gill P *Phys. Rev. A* **75** 011801(R) (2007)
48. Stoehr H et al. *Opt. Lett.* **31** 736 (2006)
49. Alnis J et al. *Phys. Rev. A* **77** 053809 (2008)
50. Corning. Specialty Materials, http://www.corning.com/specialtymaterials/
51. Matveev A N, Kolachevsky N N, Alnis J, Hänsch Th W *Kvantovaya Elektron.* **38** 391 (2008) [*Quantum Electron.* **38** 391 (2008)]
52. Allan D W *Proc. IEEE* **54** 221 (1966)
53. Numata K, Kemery A, Camp J *Phys. Rev. Lett.* **93** 250602 (2004)
54. Kolachevsky N et al. *Phys. Rev. Lett.* **92** 033003 (2004)
55. Kolachevsky N N *Kvantovaya Elektron.* **35** 207 (2005) [*Quantum Electron.* **35** 207 (2005)]

56. Karshenboim S G et al. *Zh. Eksp. Teor. Fiz.* **129** 419 (2006) [*JETP* **102** 367 (2006)]
57. Ramsey N F, in *Quantum Electrodynamics* (Ed. T Kinoshita) (Singapore: World Scientific, 1990) p. 673; *Hyp. Interactions* **81** 97 (1993)
58. Kolachevsky N et al. "Ultra-stable sub-hertz diode laser system for 1S-2S spectroscopy in atomic hydrogen", in *German – Russian Laser Symp., Lübeck, Germany, 12 – 18 April 2008*
59. Rothery N E, Hessels E A *Phys. Rev. A* **61** 044501 (2000)
60. Sengstock K et al. *Opt. Commun.* **103** 73 (1993)
61. Metcalf H J, van der Straten P *Laser Cooling and Trapping* (New York: Springer, 1999)
62. Baklanov E V, Chebotaev V P *Kvantovaya Elektron.* **4** 2189 (1977) [*Sov. J. Quantum Electron.* **7** 1252 (1977)]
63. Dudovich N, Oron D, Silberberg Y *Nature* **418** 512 (2002)
64. Marian A et al. *Phys. Rev. Lett.* **95** 023001 (2005)
65. Gerginov V et al. *Opt. Lett.* **30** 1734 (2005)
66. Akimov A V et al. "Rezonansnoe vzaimodeistvie femtosekundnogo izlucheniya s oblakom kholodnykh atomov Rb-87" ("Resonance interaction of femtosecond radiation with cloud of cold atoms Rb-87") *Zh. Eksp. Teor. Fiz.* (in print)
67. Duncan B C et al. *Phys. Rev. A* **63** 043411 (2001)